Annals of Nuclear Energy 180 (2023) 109476

Contents lists available at ScienceDirect

Annals of Nuclear Energy

journal homepage: www.elsevier.com/locate/anucene

Atmosphere homogenization induced by vertical jets in large enclosures

Rok Krpan [a,b,*], Iztok Tiselj [a,b], Ivo Kljenak [a]

[a] Jožef Stefan Institute, Reactor Engineering Division, Jamova cesta 39, SI-1000 Ljubljana, Slovenia
[b] University of Ljubljana, Faculty of Mathematics and Physics, Jadranska ulica 19, SI-1000 Ljubljana, Slovenia

ARTICLE INFO

Keywords:
Stratified atmosphere homogenization
Vertical injection
Turbulent Schmidt number
Turbulent Prandtl number
Local Froude number

ABSTRACT

To theoretically investigate atmosphere mixing in an enclosure, three experiments of interaction of a vertical air jet with a helium-rich layer performed in SPARC, PANDA and MiniPanda experimental facilities, were simulated using the URANS approach. For the purposes of this work, firstly, a local Froude number is introduced, which can be directly used in computational fluid dynamics calculations to specify the regions with possible occurrence of Kelvin-Helmholtz instability. Namely, it is shown that in these regions, turbulent diffusion is underpredicted and turbulence model fails to replicate some phenomena. Secondly, a model for dynamically prescribe turbulent Schmidt and Prandtl numbers is proposed. The proposed model improves the results in isothermal case with possible occurrence of Kelvin-Helmholtz instability, while its effects are negligible in cases with higher temperature jets with lower local Froude number values, where the conditions for the Kelvin-Helmholtz instability are not established.

1. Introduction

The study of hydrogen distribution during a severe accident in a light water nuclear reactor is important to predict the occurrence of regions in nuclear power plant (NPP) containment with high local hydrogen concentrations and flammable mixture in order to effectively install hydrogen mitigation systems. Various experiments are being performed, with the use of helium as a substitute for hydrogen, to simulate atmosphere mixing occurring in NPP containments; results are used to validate Computational Fluid Dynamics (CFD) codes in order to simulate phenomena during accidents in actual plants (Kljenak et al., 2012).

The issue of homogenization of a stratified atmosphere using a vertical gas jet is considered in the present work. Three experiments performed in different facilities are used to validate a proposed model. During the tests, the erosion of helium-rich layer in the upper part of the experimental vessels with a vertical axisymmetric air jet was observed. The first experiment considers an isothermal break-up of a stratified atmosphere in the SPARC (Spray-Aerosol-Recombiner-Combustion) large-scale test facility, located at Korea Atomic Energy Research Institute (KAERI) in Daejeon (Republic of Korea) (Na and Kim, 2018; Lee et al., 2019). The second experiment considered in the present work was performed in the PANDA experimental facility at the Paul Scherrer Institute (PSI) in Switzerland (Mignot et al., 2010). This experiment was part of the OECD SETH-2 project (2007–2010) (OECD, 2012), in which experiments on generation of stratified containment atmosphere and its mixing due to jets, sprays and natural convection were performed. The third experiment was performed in the MiniPanda experimental facility, located at ETH Zürich in Switzerland (Ritterath, 2012; Kelm et al., 2016).

The turbulent Schmidt number (Sc_t) and the turbulent Prandtl number (Pr_t) are non-dimensional numbers used in turbulence modelling to describe the turbulent transport of mass and heat, respectively. In CFD calculations of the injection of fluid from a nozzle of circular cross-section into a reservoir containing stagnant fluid of similar density, constant values of Sc_t and Pr_t are usually used. Typically, their values are based on comparisons of calculation and experimental results (Andreani et al., 2016). However, a constant value does not always provide a satisfactory agreement with experiments. In fact, values of these turbulent numbers are expected to change throughout the flow field (Ishay et al., 2015) and within the boundary layer (Koeltzsch, 2000). In the experimental study on turbulent horizontal negatively buoyant jets performed by Shao and Law (2009), the calculated Sc_t values were in the range from 0.4 to 1.0. In their experiment of horizontal stratified jet, Xu and Chen (2012) observed a strong spatial variation of Sc_t with values from 0.6 to 1.5. They also concluded that to model turbulence properly, a combination of mixing length model and eddy viscosity turbulence model is suitable.

Varying such quantities over the flow field is a way of extending the

* Corresponding author.
E-mail addresses: rok.krpan@ijs.si (R. Krpan), iztok.tiselj@ijs.si (I. Tiselj), ivo.kljenak@ijs.si (I. Kljenak).

https://doi.org/10.1016/j.anucene.2022.109476
Received 17 September 2021; Received in revised form 16 August 2022; Accepted 19 September 2022
Available online 28 September 2022

existing physical modelling but without questioning the fundamentals, that is, the hypothesis that these quantities significantly determine the behaviour of the flow. Using such an approach, models that have proved to be successful at other conditions are not negated, but extended. Several authors have proposed different models for Pr_t and Sc_t values. Yimer et al. (2002) have proposed a parabolic curve fit for Sc_t. This function is based on several turbulent round free jet experiments, which showed that Sc_t increases monotonously from a value of 0.62 on the jet axis to 0.82 on the jet edge. However, a constant average value of 0.7 is recommended for use in CFD applications involving axisymmetric free-jet flows. Sturgess and McManus (1984) suggested a formulation for Sc_t based on the $k-\varepsilon$ turbulence model. One of the model constants, was modelled using the ratio of turbulence kinetic energy production to its dissipation rate. Keistler et al. (2006) proposed a new set of transport equations for enthalpy and mean mass fraction, including variance and dissipation rate, in order to determine Sc_t and Pr_t. However, this set of equations involves 26 additional constants. Goldberg et al. (2010) proposed a method for calculating Sc_t and Pr_t values based on algebraic Reynolds stress model and Reynolds stress anisotropy. This method gives in the bulk flow a constant Sc_t value of 0.7, while in the near wall region a lower Sc_t mean value of 0.34 is obtained.

Venayagamoorthy and Stretch (2010) derived a formulation for Sc_t and Pr_t in terms of the strength of stratification (Richardson number) for homogeneous stably stratified turbulent flows. This Sc_t and Pr_t formulation was used by Abe et al. (2018), who studied two experiments performed in the MISTRA facility (CEA, France) regarding stratification break up by a buoyant jet. The simulation results of the higher injection velocity case were improved with the use of dynamic modelling of Sc_t and Pr_t. On the other hand, the erosion rate in the lower injection rate case was overpredicted, indicating that the turbulence model cannot simulate the buoyant jet adequately. The same formulation to dynamically prescribe turbulent numbers was also used in simulations of the erosion of a stable stratified atmosphere by a vertical jet from below by Abe et al. (2020). The turbulence production profiles predicted by the dynamically modelled Sc_t are similar to large-eddy simulation (LES) results, which increases the accuracy of the results. They concluded that the change of the Sc_t values plays a significant role in simulating the turbulence behaviour in the density stratification comprising the multicomponent gas mixture.

Tahmooresi and Ahmadyar (2021) used a “regional Sc_t” approach (as stated by the authors), prescribing different Sc_t values in an inclined negatively buoyant jet. Different regions were isolated using negative or positive values of turbulence buoyancy production and vertical velocity. $Sc_t = 0.8$ was prescribed in the almost jet-like region and in the outer half of the flow, $Sc_t = 0.4$ was prescribed in the additional mixing zone below the jet, and $Sc_t = 1.0$ in the region with absence of density stratification above the jet. It was observed that locally reducing Sc_t improves mixing parameters (dilution ratio) without changing the geometrical properties of the jet. On the other hand, using the lower value on the whole numerical domain led to a worse prediction of the shape of the jet. It was concluded that such local changes in Sc_t compensate the flaws of linear two-equation turbulence models.

In the present study, the interaction of a vertical axisymmetric air jet with a horizontal layer of helium-air mixture is simulated with the open-source CFD code OpenFOAM (OpenFOAM Ltd., 2021). The numerical and physical model implemented in the code used in the present work was developed, verified and validated in Krpan et al. (2021). However, the discrepancies between experimental and numerical results were in some cases considerable. In the present paper, firstly, a local Froude number is defined, which can be directly used in CFD calculations to directly assess jet characteristics. Secondly, a new model for dynamically prescribing turbulent Schmidt and Prandtl numbers is proposed and validated against experimental results.

The constrained vertical jet is described in Section 2 and experimental facilities and experiments are described in Section 3. The physical model and model for dynamically prescribe different values of turbulent Schmidt and Prandtl numbers are described in Section 4. In Section 5, the validation of the proposed model against experimental results is presented.

2. Vertical jet and light gas layer interaction

In the present section, a phenomenological description of the velocity field, induced by a vertical jet, is provided as the basis for the later presentation of the proposed model in Section 4.3. Instantaneous velocity and density fields presented in this section as illustrations of the phenomenological descriptions are taken from simulations of experiment performed in SPARC experimental facility at $t = 1000s$. The velocity values are normalized with the injection velocity.

The vertical axisymmetric jet injected in the opposite direction of the gravity considered in the present experiments is constrained in the vertical (streamwise) direction, at first with a light gas layer and later with the ceiling of the vessel. Consequently, the jet at some point changes its direction, flows downstream around the main jet and a recirculating flow is generated. Fig. 1 shows absolute value of instantaneous vertical velocity field in logarithmic scale and streamlines in a typical constrained vertical jet. Regarding the vertical velocity, the following flow regions can be defined:

A. upward flowing main jet,
B. downward flowing returning jet,
C. quiescent environment.

Let us define a Cartesian coordinate system with origin located in the centre of injection and z axis pointing upwards (in the opposite direction of gravity). Fig. 2 (left) shows a vertical velocity radial (x-direction) profile 2 m above the injection. However, the radial profile in a typical fully-developed axisymmetric jet is similar regardless the distance from the injection. The velocity is highest in the axis of the main upward flowing jet directly above the injection. Further away from the jet axis, the vertical velocity decreases, becomes zero on the boundary between the main jet and the downward flowing returning jet, and reaches its minimum value in the axis of the returning jet. Further on, the vertical velocity increases back to zero in the quiescent environment. Fig. 2 (right) shows the vertical velocity vertical profile in the jet axis. The velocity decreases and when the jet reaches either a layer consisting of light gas or the ceiling, it becomes zero.

Fig. 3 shows the density field (Fig. 3 left) and the vertical density gradient (Fig. 3 right) in an isothermal vertical jet with a layer of light gas above. The figure is taken at $t = 1000s$ when enough helium is already brought to lower atmosphere and such density gradients are present also in the proximity of the injection. In the vertical direction in the axis of the jet, the density is highest at the injection pipe outlet, and decreases when moving higher, meaning the density gradient is negative. The gradient has the highest value (in the absolute sense) at the interface between the jet and the light gas layer. In the radial direction from the axis, the density gradient depends on the entrainment of the light gas. Where the gradient is negative, the mass fraction of light gas increases, and vice versa, where the density gradient is positive, the mass fraction decreases.

The behaviour of a typical vertical jet in an environment with a density stratification can be characterized by the Froude number (Fr) that is defined as the ratio of inertial forces (jet's momentum) to the buoyancy forces (Paladino et al., 2008b):

$$Fr^2 = \frac{u^2}{g \cdot D \frac{(\rho_0 - \rho_{amb})}{\rho_0}} \tag{1}$$

where u, g, D, ρ_0 and ρ_{amb} are vertical jet representative velocity, gravitational acceleration, jet representative diameter, jet density and density of the ambient atmosphere, respectively.

With the means of Fr, the behaviour of the jet in different regions can

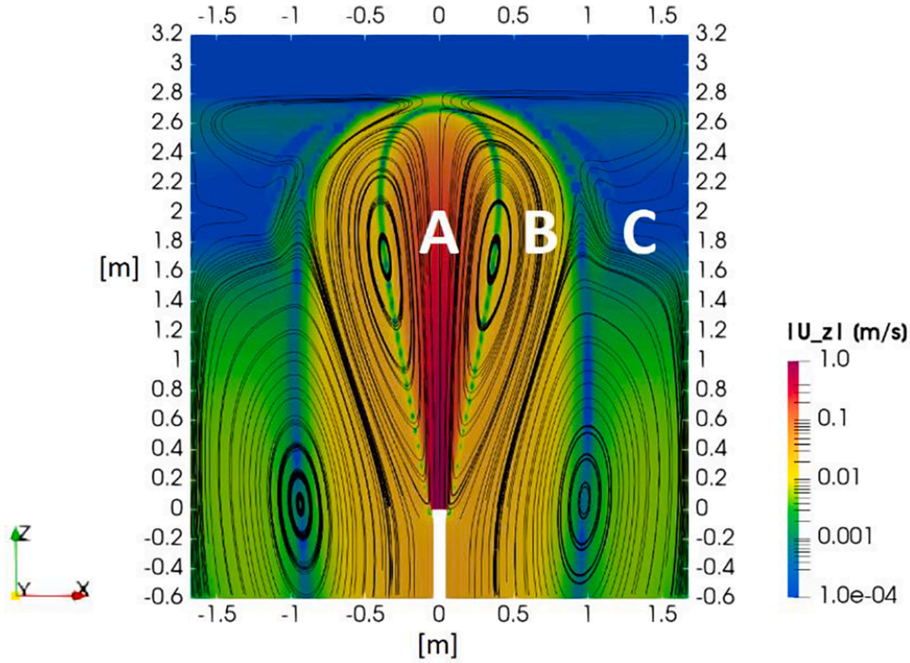

Fig. 1. Absolute value of vertical velocity field (logarithmic scale) and streamlines in a constrained vertical jet.

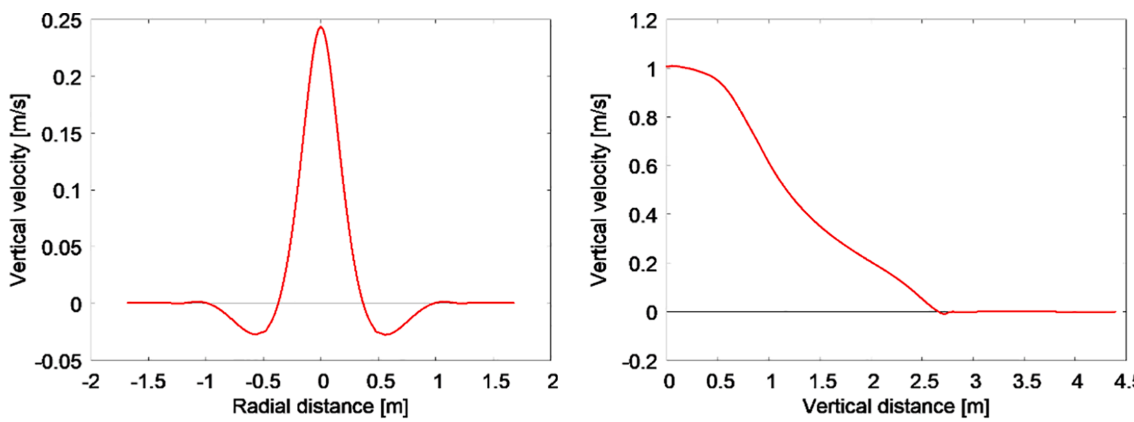

Fig. 2. Vertical velocity radial profile (left) and vertical velocity vertical profile (right).

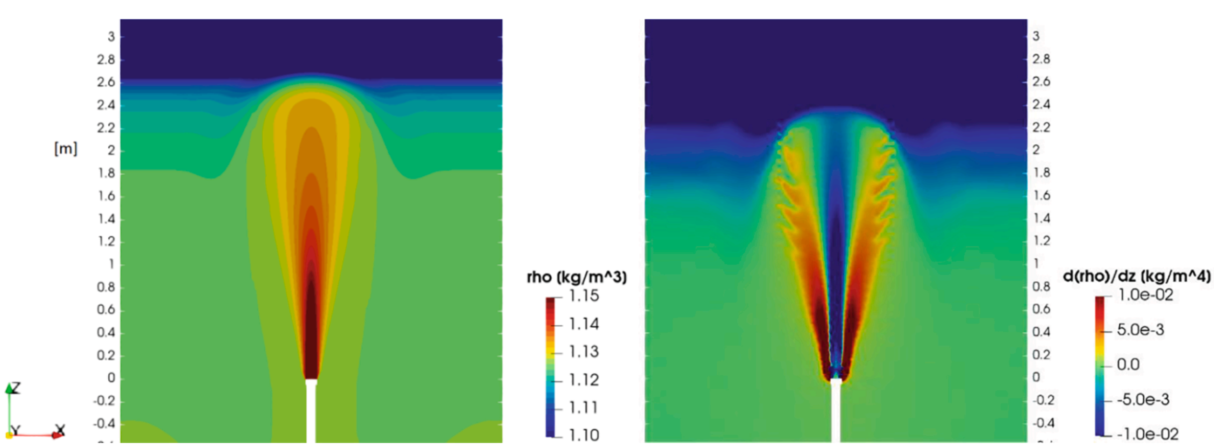

Fig. 3. Density field (left) and vertical density gradient (right).

be characterized. If the injection velocity and density are inserted in Eq. (1), the calculated Fr expresses the behaviour of the jet at the injection. In the same way, the interaction between a vertical jet and a light gas layer can be characterized by means of the interaction Froude number (Fr_{int}). Fr_{int} describes the initial conditions at the interface between the jet and light gas layer where the erosion takes place, and is defined as (Kelm et al., 2016):

$$Fr_{int}^2 = \frac{u_{int}^2}{g \cdot D_{int} \frac{(\rho_0 - \rho_{layer})}{\rho_0}} \tag{2}$$

where u_{int}, D_{int} and ρ_{layer} are the velocity and the jet diameter at the interface, and the light gas layer density, respectively. If $Fr_{int} < 1$, buoyancy forces dominate the flow and the erosion process is slow, since the jet erodes the layer almost without any penetration. If Fr_{int} 1, the inertial and buoyancy forces are nearly equal. If $Fr_{int} > 1$, the mixing is driven by the momentum, the vertical jet deeply penetrates in the light gas layer and the erosion is fast. Fr_{int} is used to scale experiments performed in different experimental facilities. Usually, it is calculated using only initial parameters, without considering the layer with decreasing helium concentration (Fig. 6) and the actual jet velocity and density in the interaction region (Kelm et al., 2016). Besides, it neglects the temporal changes in the density of the jet caused by the entrainment of the light gas.

The Froude number is calculated using the conditions at two specific locations and is expressed as a single parameter. As such it is not valid for the entire computational domain and thus it cannot be directly used in CFD calculations, where the fluid properties are locally and time dependent. For the purposes of the present work, a local Froude number (Fr_l) is defined, which uses local vertical velocity (u_z), local density (ρ) and vertical density gradient:

$$Fr_l^2 = \frac{u_z^2}{g \cdot D^2 \frac{1}{\rho} \left| \frac{\partial \rho}{\partial z} \right|} \tag{3}$$

where D^2 is a constant with a unit ($D^2 = 1m^2$). Fr is in general considered to be always positive, and consequently the absolute value of the density gradient must be taken into account in Fr_l (Eq. (3)). The behaviour of Fr_l in a vertical constrained jet is discussed in Section 5.

In cases considering the flow of two or more fluids, Kelvin–Helmholtz instability may appear. When two fluids, separated by an interface, move with different velocities, the interface is submitted to shear. The interface becomes unstable and periodic large-scale vortices may be generated. Kelvin-Helmholtz instabilities typically appear when the velocity difference of two fluids across the interface exceeds a critical value (Δu_c) (Štrubelj and Tiselj, 2005):

$$\Delta u_c^2 \geq 2 \frac{\rho_1 + \rho_2}{\rho_1 \rho_2} \sqrt{(\rho_1 - \rho_2) g \sigma} \tag{4}$$

where ρ_1, ρ_2, g and σ are density of the first fluid, density of the second fluid, gravitational acceleration and surface tension coefficient, respectively.

However, Kelvin–Helmholtz instability may appear also in continuous flow of a single fluid in the presence of a velocity shear. It can be observed in Fig. 1 that in the constrained vertical jet, a recirculation flow is generated, and a shear flow is most prominent near the inlet. Furthermore, due to the different content of the light gas, densities of the upwards and downwards flowing jets are different. Fig. 4 shows vertical velocity (left) and density (right) radial (x-direction) profiles 0.1 m above the injection at t = 1000 s.

In our case, the shear flow is generated by a single fluid with a slightly different density and the surface tension cannot really be assessed. Consequently, for the assessment of ΔU_c, the same value of the surface tension was used as in Štrubelj and Tiselj (2005), i.e. $\sigma = 0.04$ N/m. Considering the maximum and minimum density values from Fig. 4 ($\rho_1 = 1.16 \mathrm{kg/m^3}$ and $\rho_2 = 1.12 k\mathrm{g/m^3}$) in Eq. (4), the assessed $\Delta u_c \geq 0.66 \mathrm{m/s}$. In Fig. 4 left, the maximum and minimum values of the velocity are $u_z = 3.02 \mathrm{m/s}$ and $u_z = -0.1 \mathrm{m/s}$, respectively. Such velocity difference of $\Delta u_z = 3.12 \mathrm{m/s}$ exceeds the assessed Δu_c, and consequently the occurrence of Kelvin-Helmholtz instability is possible.

3. Experimental facilities and experiments used for model validation

Experimental facilities considered in the present work are designed as a single vessel or a system of vessels in order to study physical phenomena during the atmosphere homogenization process. The main purpose of these experiments was to observe the interaction of a vertical air jet with a previously established horizontal layer of helium-air mixture in the upper parts of the vessels. The initial and boundary conditions of the tests used for model validation in the present work are listed in Table 1. The interaction Froude number (Fr_{int}) describes the

Table 1
Boundary and initial conditions for simulated tests.

Experiment	Position of injection line	Helium content [vol. %]	Injection flow rate [g/s]	Interaction Froude number	Initial injection density ratio at pipe exit
SPARC	centre	30	28	0.51	1
PANDA	near wall	45	15	0.75	0.95
MiniPanda	near wall	100	1.51	1.3	0.84

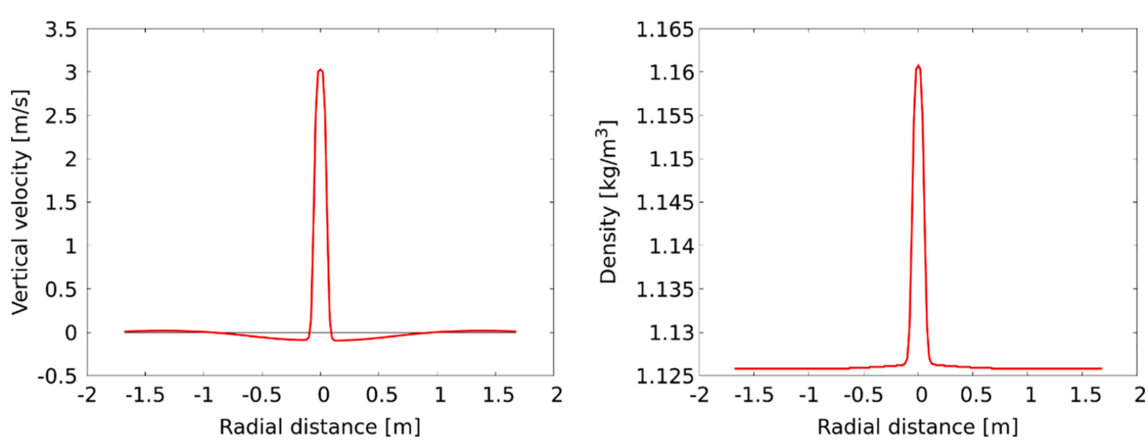

Fig. 4. Vertical velocity (left) and density (right) radial profiles.

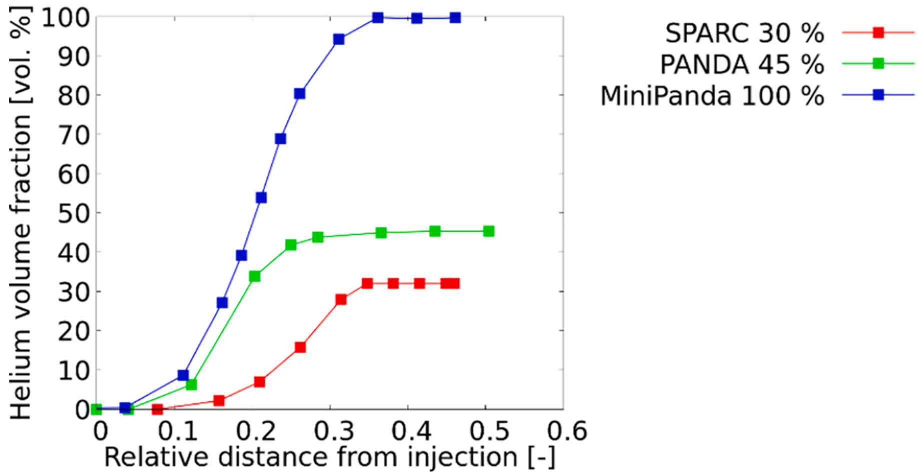

Fig. 5. Initial helium distribution profiles for different experiments (Mignot et al., 2010; Na and Kim, 2018; Ritterath, 2012).

conditions at the interface between the jet and the light gas layer where the erosion takes place, and is defined using Eq. (2). Initial helium volume fraction vertical distribution profiles in the experiments are shown in Fig. 5. On x-axis is relative distance from the injection, $(z - H_{inj})/H_{vessel}$, where z, H_{inj} and H_{vessel} are vertical coordinate, height of the injection and vessel height.

3.1. SPARC experimental facility

The SPARC test facility (Fig. 6) consists of a single cylindrical vessel with a volume of 80 m^3 (Na and Kim, 2018; Lee et al., 2019). Before the experiment, a 1.5 m thick layer with 30 vol% of helium (the rest was air) was established in the upper part of the vessel (Fig. 6). During the experiment considered in the present work, the helium-air layer was eroded with an axisymmetric vertical air jet with a mass flow rate of 28 g/s. The jet with a diameter of 0.1 m was injected at the axis of the vessel at an elevation of 5.15 m and had the same temperature as the previously established atmosphere. The constant pressure in the vessel was maintained using an open nozzle at the bottom of the vessel (Na and Kim, 2018).

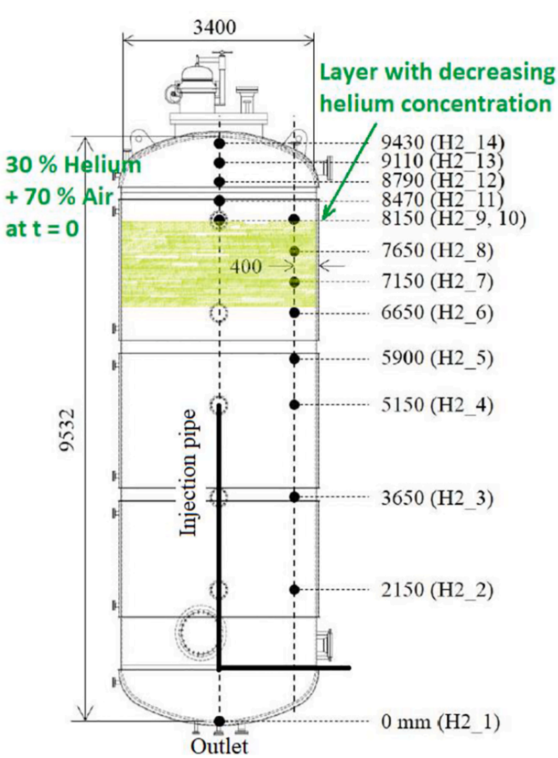

Fig. 6. Schematic of SPARC experimental facility and sampling positions (Na and Kim, 2018).

3.2. PANDA experimental facility

The part of the PANDA experimental facility that was used for the experiment considered in the present work consists of two cylindrical vessels and an interconnecting pipe, with a total volume of 183 m^3 (Fig. 7 left). Each vessel has a height of 8.0 m and a diameter of 3.96 m with a volume of 89.9 m^3. The injection pipe is positioned 0.5 m away from the wall and has a diameter of 0.075 m. In the experiment considered in the present work, the initial pressure and temperature in the vessel were 1 bar and 20 °C, respectively.

Before the test, a 2 m thick layer of helium and air was established in the upper part of one of the vessels, as shown in Fig. 7 (left). During the experiment, the helium rich layer was eroded with an air jet with a mass flow rate of 15 g/s at a temperature 30 °C. The constant pressure in the vessel was maintained with an open nozzle at the top of the second vessel. Fig. 7 (right) shows sampling positions, from which results are compared in this paper. A more detailed description of the PANDA facility and experiments can be found in works of Paladino et al. (2008a) and Mignot et al. (2010).

3.3. MiniPanda experimental facility

MiniPanda is a 1:4 scaled-down model of the PANDA facility, with a total volume of 2.875 m^3 (Ritterath, 2012). Each vessel has a height of 2 m and a diameter of 1 m (Fig. 8). The injection pipe with a diameter of 0.018 m is positioned 0.125 m away from the wall. The constant pressure in the vessel is maintained with a vent opening at the top of the second vessel. A more detailed description of the MiniPanda facility can be found in the work of Ritterath (2012).

During the experiment considered in the present work, approximately 0.5 m thick layer of pure helium was eroded with vertical air jet with a mass flow rate of 1.51 g/s and temperature of 80 °C. The initial atmosphere temperature was 25 °C. The entire experiment was performed at constant pressure 1 bar.

4. Numerical model

Numerical simulations were performed with the OpenFOAM CFD code, version 1812 (OpenCFD Ltd, 2021). To simulate the transient mixing process, the Unsteady Reynolds Averaged Navier Stokes

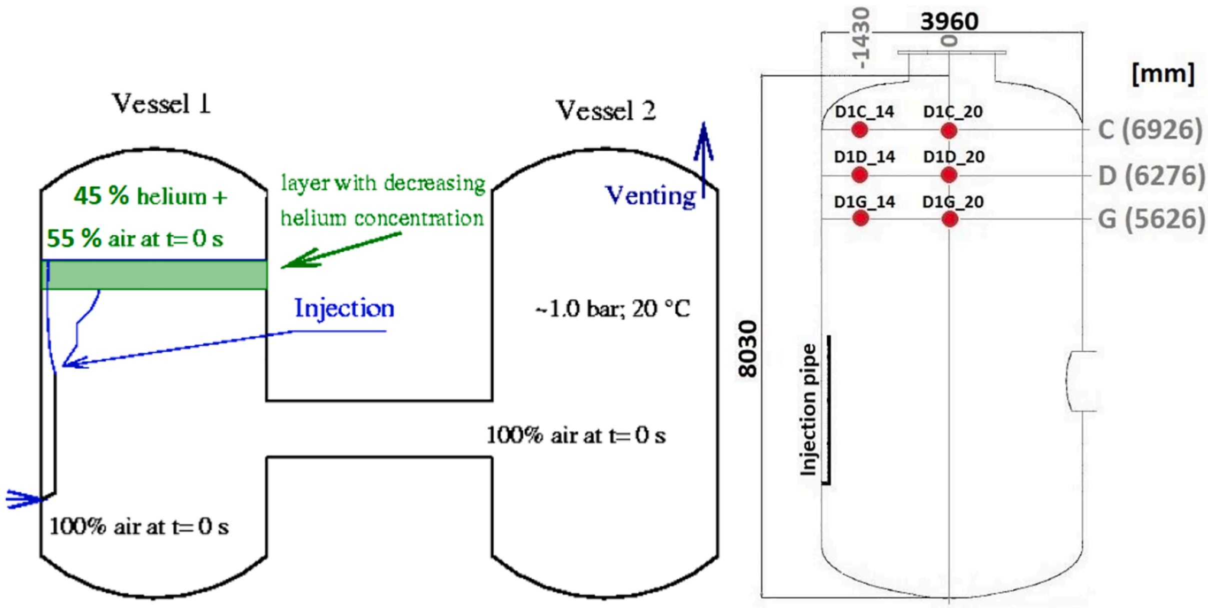

Fig. 7. Schematic of PANDA facility and initial conditions (left) and sampling positions (right) (Paladino et al., 2008a, 2008b).

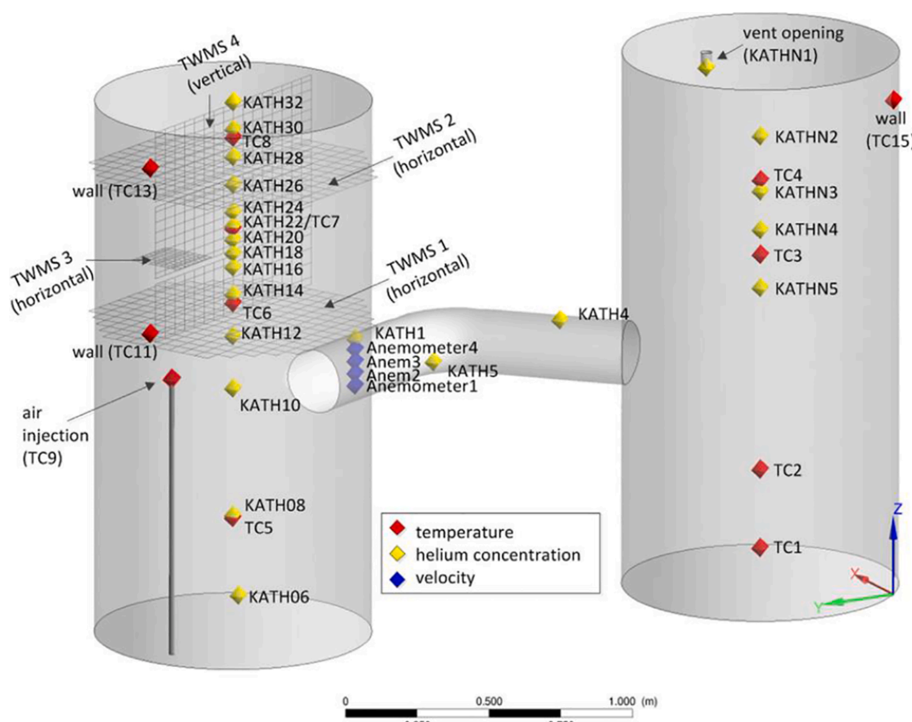

Fig. 8. Schematics and sampling positions in MiniPanda facility (Kelm et al., 2016).

(URANS) approach was used. An adaptive time step (approx. 0.001 s) was used, to sustain a Courant-Friedrichs-Lewy (CFL) number of less than 0.5 in all cells. In our simulations, a second-order accurate finite volume discretization scheme (Gaussian integration) was specified with second-order interpolation scheme. The temporal term was discretized using a first-order implicit differencing Euler scheme (OpenCFD Ltd., 2021). A pressure-implicit split-operator (PISO) algorithm was used to iteratively couple the flow equations. This modelling approach has already been applied and validated in earlier work (Krpan et al., 2021).

In order to describe the mixing process in the present work with the best accuracy, entire experimental facilities, described in Section 2, were considered as computational domains, without any geometrical simplifications. The same numerical meshes were used for the PANDA and SPARC facilities as in the mentioned earlier work (Krpan et al., 2021), where a detailed analysis of mesh convergence was performed. As to the MiniPanda facility, due to the similar conditions, an additional separate analysis of mesh convergence was not deemed necessary.

4.1. Governing equations

The atmosphere in the vessel was considered as a compressible mixture of ideal gases. The erosion and mixing process was modelled as a two-component single-phase flow, where the solved single continuity equation was:

$$\frac{\partial \rho}{\partial t}+\frac{\partial \rho u_j}{\partial x_j}=0 \tag{5}$$

where ρ, t and u are density, time and velocity, respectively. The common momentum equation used was:

$$\frac{\partial \rho u_i}{\partial t}+\frac{\partial}{\partial x_j}(\rho u_i u_j) = -\frac{\partial p}{\partial x_i}+\frac{\partial}{\partial x_j}\left((\mu+\mu_t)\left(\frac{\partial u_i}{\partial x_j}+\frac{\partial u_j}{\partial x_i}\right)\right)-g_k x_k \frac{\partial \rho}{\partial x_i} \tag{6}$$

where p, μ, μ_t and g are pressure, dynamic and eddy viscosity (momentum eddy diffusivity), and gravitational acceleration, respectively. The helium mass fraction, Y_{He}, was calculated using the convection–diffusion equation:

$$\frac{\partial \rho Y_{He}}{\partial t}+\frac{\partial}{\partial x_j}(\rho u_j Y_{He}) = \frac{\partial}{\partial x_j}\left(\left(\rho D+\frac{\mu_t}{Sc_t}\right)\frac{\partial Y_{He}}{\partial x_j}\right) \tag{7}$$

where D and Sc_t are diffusion coefficient and turbulent Schmidt number, respectively. The convection–diffusion equation was solved only for helium, while the air mass fraction was calculated using $\sum_{i=1,2} Y_i = 1$. The total energy equation used was:

$$\frac{\partial \rho h}{\partial t}+\frac{\partial}{\partial x_j}(\rho u_j h)+\frac{\partial \rho K}{\partial t}+\frac{\partial}{\partial x_j}(\rho u_j K)-\frac{\partial p}{\partial t} = \frac{\partial}{\partial x_j}\left(\left(\frac{\mu}{Pr}+\frac{\mu_t}{Pr_t}\right)\frac{\partial h}{\partial x_j}\right)-\sum_i\left(\frac{\partial}{\partial x_j}\left(h_i\cdot\left(\rho D+\frac{\mu_t}{Sc_t}\right)\right)\frac{\partial Y_i}{\partial x_j}\right)+\rho g_k u_k \tag{8}$$

where h, K, Pr, Pr_t and h_i are enthalpy, kinetic energy, Prandtl number, turbulent Prandtl number and gas species enthalpy, respectively.

4.2. Turbulence modelling

Linear two-equation eddy viscosity models are currently state-of-the-art turbulence models in solving problems related to mixing in large enclosures. In these models, two additional transport equations are solved: a transport equation for turbulence kinetic energy (k), and a transport equation for turbulence kinetic energy dissipation (ε).

The Launder and Spalding k-ε turbulence model (Launder and Spalding, 1974) was used in the present work:

$$\frac{\partial(\rho k)}{\partial t}+\frac{\partial(\rho k u_j)}{\partial x_j}=\frac{\partial}{\partial x_j}\left[\left(\mu+\frac{\mu_t}{\sigma_k}\right)\frac{\partial k}{\partial x_j}\right]+P+B-\rho\varepsilon \tag{9}$$

$$\frac{\partial(\rho \varepsilon)}{\partial t}+\frac{\partial}{\partial x_j}(\rho \varepsilon u_j)=\frac{\partial}{\partial x_j}\left[\left(\mu+\frac{\mu_t}{\sigma_\varepsilon}\right)\frac{\partial \varepsilon}{\partial x_j}\right]=c_{1\varepsilon}\frac{\varepsilon}{k}(P+c_{3\varepsilon}B)-c_{2\varepsilon}\rho\frac{\varepsilon^2}{k} \tag{10}$$

B represents the additional production and dissipation of turbulence kinetic energy in k and ε equations due to buoyancy and was modelled as (Henkes et al., 1991):

$$B=-\frac{3}{2}\frac{\mu_t}{Pr_t}\frac{1}{\rho}g_i\frac{\partial \rho}{\partial x_i} \tag{11}$$

The default values of the turbulence model constants were used: $C_\mu = 0.09, C_{1\varepsilon} = 1.44, C_{2\varepsilon} = 1.92, C_{3\varepsilon} -0.33, \sigma_k = 1.0$ and $\sigma_\varepsilon = 1.3$. The turbulence in the near-wall region was treated using wall functions. In simulations performed with constant values of turbulent numbers, 0.85 was prescribed to Sc_t and Pr_t.

4.3. Dynamic turbulent Schmidt and Prandtl number model

The turbulent Schmidt number (Sc_t) and the turbulent Prandtl number (Pr_t) are two non-dimensional numbers used in the convection–diffusion equation (Eq. (7)) and in the total energy equation (Eq. (8)). Furthermore, these parameters are also included in the production and dissipation of turbulence kinetic energy due to buoyancy (Eq. (11)). Sc_t and Pr_t are implicitly included in the calculation of density and enthalpy gradients, which affect the velocity and turbulence fields. Sc_t is defined as the ratio of momentum eddy diffusivity (ν_t) to mass eddy diffusivity (D_t), and Pr_t is defined as the ratio of ν_t to thermal eddy diffusivity (α_t) (Davidson, 2019):

$$Sc_t=\frac{\nu_t}{D_t} \tag{12}$$

$$Pr_t=\frac{\nu_t}{\alpha_t} \tag{13}$$

where $\nu_t = \mu_t/\rho$. In other words, these numbers describe the ratio of the rates of turbulent transport of momentum (momentum diffusion) to the turbulent transport of mass (turbulent mass diffusion) or heat (turbulent heat diffusion). Usually, constant values of these two parameters are used and their values are specified based on comparison of calculation and experimental results (Andreani et al., 2016). However, a constant value does not always provide a satisfactory agreement with experiments.

Venayagamoorthy and Stretch (2010) derived a correlation between Sc_t (or Pr_t) and stratification strength, which can be characterized with the gradient Richardson number (Ri_g):

$$\frac{Sc_t}{Sc_{t0}}=\exp\left(-\frac{Ri_g}{Sc_{t0}\Gamma_\infty}\right)+\frac{Ri_g}{R_{f\infty}Sc_{t0}} \tag{14}$$

where Sc_{t0}, Γ_∞ and $R_{f\infty}$ are default Sc_t value and two constants, where $\Gamma_\infty = 1/3$ and $R_{f\infty} = 1/4$. Gradient Richardson number (Ri_g) is defined as:

$$Ri_g=\frac{N^2}{S^2} \tag{15}$$

where N^2 is buoyancy frequency (or Brunt-Väisäla frequency) ($N^2 = (-g/\rho_0)(d\rho/dz)$), and S is the mean shear rate ($S = du/dz$). Ri_g is considered to be always positive. A negative value of N^2 (i.e. complex N) indicates unstable density gradients with active convective overturning. Under such circumstances the magnitude of negative Ri_g is not generally of interest (Turner, 1973). Despite the Ri_g is based on global quantities (Shih et al., 2000; Venayagamoorthy and Stretch, 2010), it was used in Abe et al. (2020) to prescribe different Sc_t values locally.

As discussed in Section 2, in atmosphere homogenization experiments the occurrence of Kelvin-Helmholtz instability is possible, and as shown in the next section, some simulations capture oscillations in the velocity field which are similar to Kelvin-Helmholtz instability. This results in decreased erosion rate and the atmosphere homogenization is reached later than observed in the experiment.

The region with possible occurrence of Kelvin-Helmholtz instability exists especially near the inlet where the velocity difference between the upward and downward flowing jets is the highest. Furthermore, besides shear flow and velocity gradient, also a density difference (density gradient) is important. Fig. 9 shows vertical density gradient field (left) and the Fr_l field (right) calculated with Eq. (3). The figure is taken from the simulations of the experiment performed in the SPARC experimental facility at $t = 1000$ s. The white line represents $u_z = 0$m/s. It can be seen that a region with high shear velocity ($u_z = 0$m/s) next to the inlet can be also distinguished by the high value of the density gradient. When moving further in the radial direction away from the axis of the jet, the density gradient approaches zero, while Fr_l value increases. Here, u_z is negative.

Regarding the high value of Fr_l and the negative u_z in the vertical constrained jet, we propose to dynamically prescribe different Sc_t and Pr_t values in different regions. In the proposed model, the same Sc_t and Pr_t values are used in the simulations, and consequently, both of these numbers are prescribed according to the following equation:

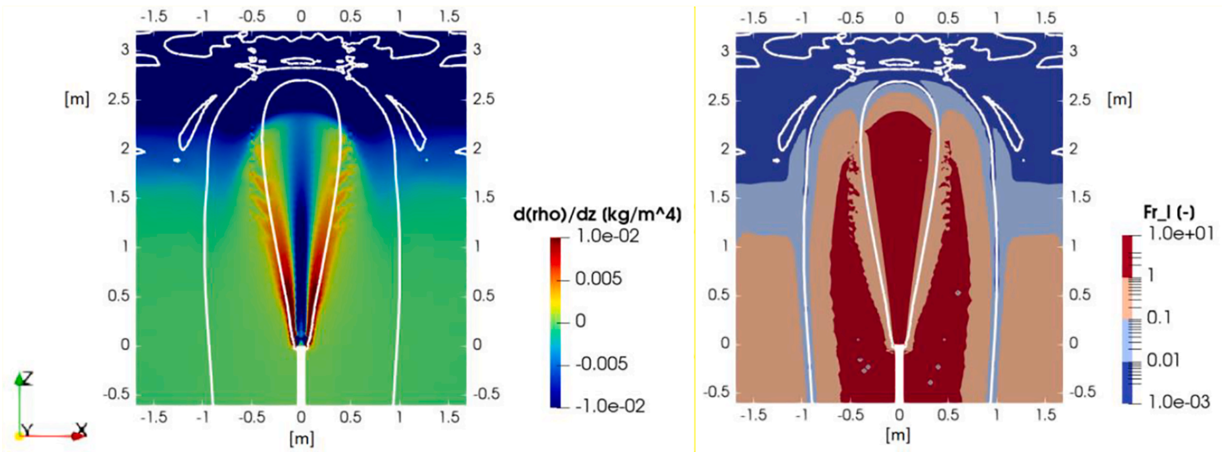

Fig. 9. Vertical density gradient field (left) and Fr_l field (right). White line represents $u_z = 0\mathrm{m/s}$.

$$Sc_t = Pr_t = Sc_{t,min} + \frac{1}{2}\left(Sc_{t,max} - Sc_{t,min}\right)\left\{1 + \tanh\left[c_{k,1} + Fr_l^2 \cdot \frac{\max(|u|)}{u_z}\right]\right\} \quad (16)$$

where $\mathrm{Sc_{t,min}}, \mathrm{Sc_{t,max}}, c_{k,1}, \max(|u|)$ and u_z are the minimum and maximum Sc_t values prescribed inside the computational domain, a model constant, the maximal velocity magnitude inside the computational domain (injection velocity) and the local vertical velocity (in the opposite direction of gravity), respectively.

Fig. 10 shows the vertical velocity in the axis of the jet 1.0 m above the injection, and the absolute values of the product of $Fr_l^2 \max(|u|)/u_z$ (Eq. (16)) in the region with possible occurrence of Kelvin-Helmholtz instability beside the inlet at $x = 0.3$ m and $z = 0.1$ m. The transient is taken from SPARC simulation, when the light gas layer was still present and the atmosphere was not homogenized yet. It can be observed that, when the absolute value of the product reaches 5, the velocity decreases and starts oscillating. Over the entire transient presented in the figure, velocity oscillations in the range of 0.25 m/s can be seen, and the product value rarely descends below 5.

The value of the constant $c_{k,1}$ in the Eq. (16) sets the setpoint at which the value of the product of Fr_l^2 and the normalized velocity $(\max(|u|)/u_z)$ is taken into account. As discussed, $c_{k,1} = 5$ leads to desired behaviour of the proposed model. Namely, keeping high Sc_t and Pr_t values in the main jet, while reducing the values in the proximity of the injection.

The hyperbolic tangent function is selected because it smoothly connects upper and lower $\mathrm{Sc_t}$ and Pr_t values, regardless the extreme values of gradients during simulations. The function written in such form acts as an "if" function. Namely, where function arguments are negative, it prescribes lower $\mathrm{Sc_t}$ and Pr_t values and vice versa. Furthermore, in the interval of small arguments around zero the result of hyperbolic tangent is continuously differentiable, which avoids numerical instabilities.

This proposed model was used to dynamically prescribe both turbulent numbers (Sc_t and Pr_t), and the applied values were the same. $Sc_{\mathrm{t,min}}$ and $Sc_{\mathrm{t,max}}$ were prescribed according to the values observed in the experiments and used in other CFD studies (Shao and Law, 2009; Xu and Chen, 2012; Andreani et al., 2016; Tahmooresi and Ahmadyar, 2021). Parameters listed in Table 2 are used in all cases simulated with the dynamic model (Eq. (16)) presented in the next sections.

5. Results and discussion

5.1. SPARC experiment

Fig. 11 shows time-dependent helium volume fractions at several representative locations in the SPARC facility. Results obtained with constant Sc_t value, the Sc_t model by Venayagamoorthy and Stretch (2010) (Eq. (14)), and with the proposed dynamic Sc_t model (Eq. (16))

Table 2
Dynamic turbulent Schmidt number model constants.

Constant	$Sc_{t,min}$	$Sc_{t,max}$	$c_{k,1}$
Value	0.4	0.85	5

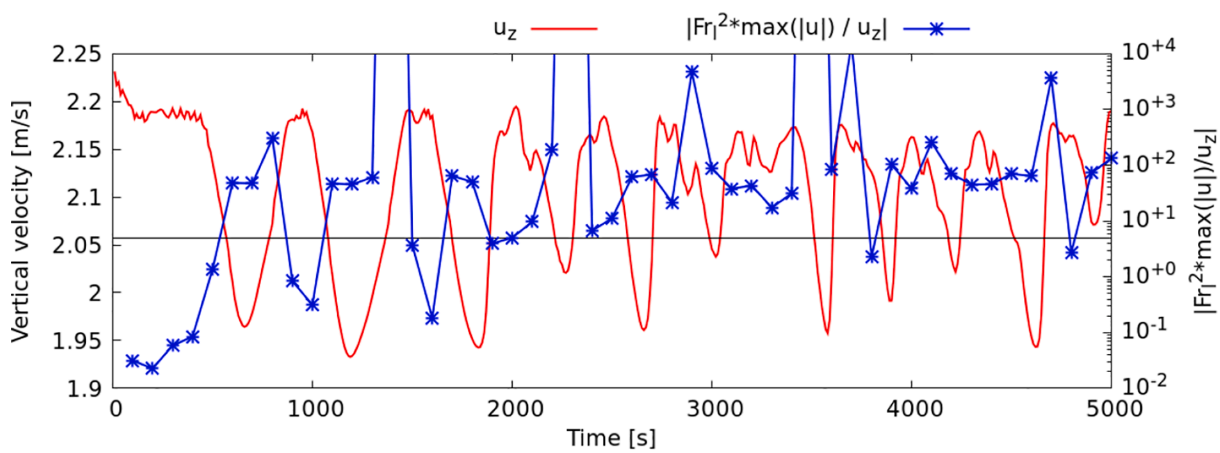

Fig. 10. Vertical velocity in the axis of the jet at $z = 1.0$ m, and absolute value of $Fr_l^2 \cdot \max(|u|)/u_z$ at $x = 0.3$ m and $z = 0.1$ m.

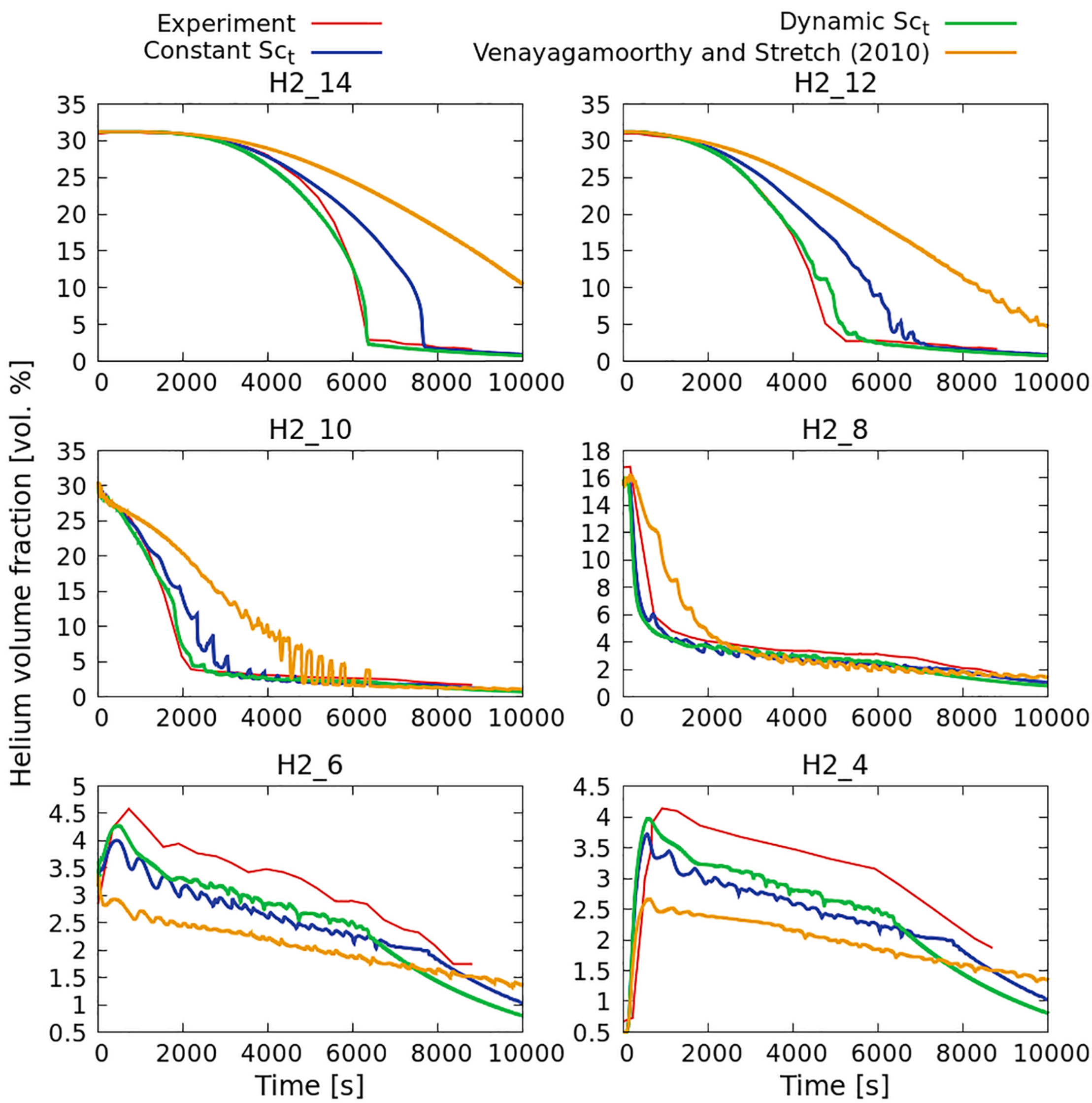

Fig. 11. SPARC experiment: helium volume fractions at different measuring locations (for sampling positions see Fig. 6).

are compared to experimental results. It can be observed that the formulation proposed by Venayagamoorthy and Stretch (2010) does not replicate well the experiment performed at isothermal conditions, and the atmosphere homogenization is even slower than with the constant Sc_t value.

If we first consider helium concentrations at lower measuring positions near the vessel wall (H2_4, H2_6 and H2_8), we may notice, that there is not much difference between results obtained with constant Sc_t and those obtained with the proposed dynamic Sc_t, and that they both match experimental results quite well (although discrepancies at H2_4 and H2_6 may seem large, the difference is still only 1 vol%).

At measuring positions directly above the injection, that is H2_10, H2_12 and H2_14 the experimental concentrations and concentrations obtained with constant Sc_t value at first coincide. Later, the simulated erosion rate, i.e., the rate of concentration decrease, is reduced and final concentration values are thus reached later than observed in the experiment. On the other hand, the results given by the proposed Sc_t model are significantly improved. When compared to experimental results, the erosion rate is the same and the atmosphere homogenization is reached simultaneously as in the experiment. In total, the agreement obtained with the proposed dynamic model is in line with the reasoning, presented in the introduction, that the new model represents an extension that much better replicates the experiments in some conditions.

Fig. 12 shows helium volume fraction vertical profiles at $t = 5000$s. As discussed before, the helium layer erosion by the default model and by the formulation by Venayagamoorthy and Stretch (2010) is slower than in the experiment. On the other hand, the height of the light gas layer is properly predicted by the proposed model.

All simulations capture oscillations of the helium volume fraction, which are not observed in the experimental results and neither in PANDA and MiniPanda simulations presented in the next sections. Fig. 13 shows vertical velocity values at different heights directly above the injection. The upper curves represent the vertical velocity at z = 7 m, the middle curves at z = 7.5 m, and the lowest curves at z = 8 m. In the results obtained with constant Sc_t value, oscillations in the range of 0.3 m/s can be observed. The velocity starts oscillating when the returning descending plume interacts with the main jet at the injection point. This results in diminished jet penetration depth, and the erosion process is reduced. Such velocity oscillations might indicate the presence of Kelvin–Helmholtz instability, which the CFD model is unable to properly resolve. In the experiment, Kelvin–Helmholtz instability could be measured using the particle image velocimetry technique, but since there are currently no such measurements of the considered experiment available, this remains an open question. On the other hand, the velocity

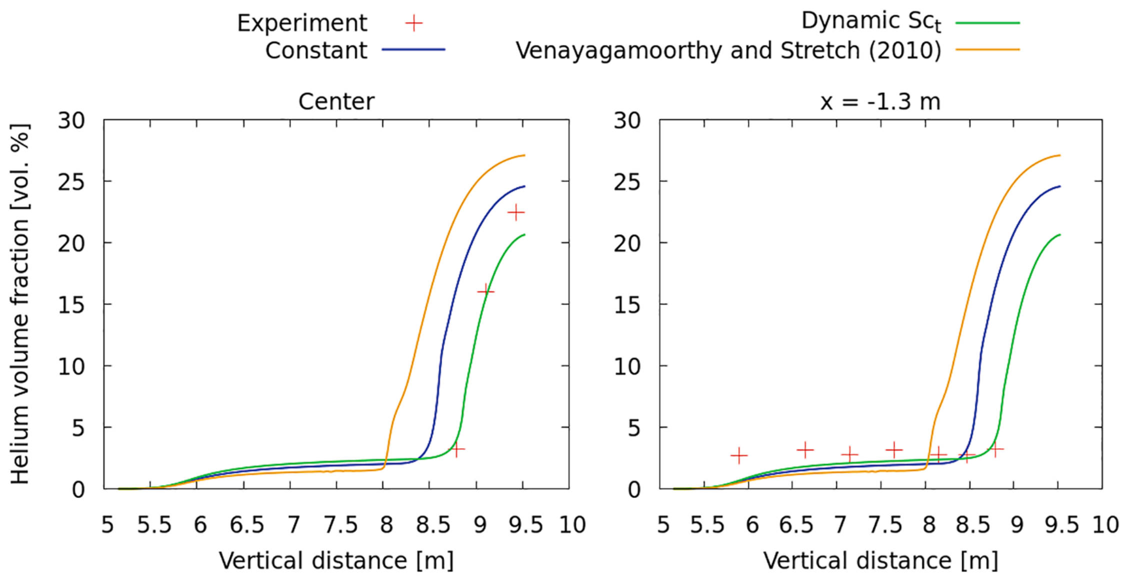

Fig. 12. SPARC experiment: helium volume fraction vertical profiles at $t = 5000s$ in center (left) and at $x = 1.3\mathrm{m}$ (right).

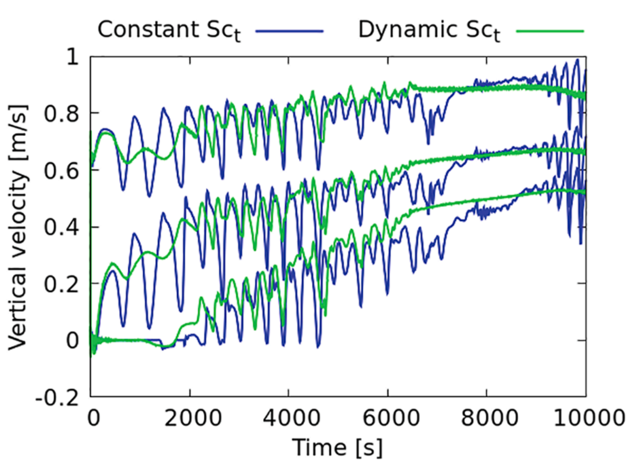

Fig. 13. Vertical velocity computed directly above injection (x = 0 m) at z = 7 m (top curve), z = 7.5 m (middle curve) and z = 8 m (bottom curve).

oscillations are reduced in the simulations with the dynamic Sc_t model proposed in this work. In this case, the velocity oscillates due to the transversal oscillations of the jet, as shown in Fig. 14.

In all PANDA and MiniPanda simulations, the jet gradually progresses upwards without any perturbations. On the other hand, in SPARC simulations with the default model, the velocity oscillates vertically and also transversally (Krpan et al., 2021). During the attempts to suppress the jet swerving motion and to improve the results, different numerical approaches were tested, but the oscillations persisted. Different parts of the numerical domain were refined and/or omitted, different time steps were chosen (CFL from 0.1 to 10), different numerical schemes (first order, second order, combined) and numerical solvers were used, and also different initial and boundary conditions were prescribed without any improvement. Since the first order schemes tend to be more diffusive than the numerical schemes of second order, the use of first order time scheme in combination with first order discretization scheme should stop the oscillations. For this reason, we may conclude that these oscillations are generated by the default implemented physical model. Furthermore, the period of the oscillations is initially almost 1000 s (Fig. 13) which is unlikely to be caused by the numerical methods.

Fig. 14 shows the velocity field obtained with the proposed dynamic Sc_t model (Eq. (16)) at different times. Although some asymmetry can be seen, the jet does not oscillate vertically, as observed in the results obtained with constant Sc_t (Krpan et al., 2021). Consequently, the erosion of the light gas layer is predicted better, and the atmosphere homogenization process is as observed in the experiment.

The Sc_t field given by Venayagamoorthy and Stretch (2010) formulation (Eq. (14)) obtained in the simulation of the experiment performed in the SPARC facility is shown in Fig. 15. This correlation maintains the lowest value $Sc_t = 0.85$ in the jet and near the vent, while a higher value, $Sc_t = 20$, is prescribed in other parts of the numerical domain. A threshold value of $Sc_t = 20$ was set as in Abe et al. (2020). As it was experimentally discovered (Shao and Law, 2009; Xu and Chen, 2012), such Sc_t behaviour in a jet is not always the case, and the value can also decrease to $Sc_t = 0.4$.

The reason for the erosion rate decrease observed in the simulations (Fig. 11), is in the isothermal conditions, at which the experiment is performed, and higher injection flow rate, which may generate the Kelvin-Helmholtz instability. Due to the same initial temperature and composition of the jet and the atmosphere in the proximity of the injection, their densities are the same (Table 1). Later, when the air in the proximity of the injection is partially mixed with helium, the jet's density becomes higher than the density of the surroundings. The negative buoyancy force in the jet at some point becomes dominant, which dampens the jet and also decreases the erosion rate. As discussed in Section 2, Fr_l can be directly used in numerical simulations to characterize the local behaviour of the jet. Fig. 16 shows the calculated Fr_l field in the SPARC simulations. $Fr_l > 1$ may be seen firstly in the proximity of the injection (at $t = 1000s$), and later over the entire numerical domain. Compared with the results from the next sections, such Fr_l behaviour is the reason that the common default physical model (implemented in the OpenFOAM CFD solver) is not capable of dealing with such perturbations and without any modification it is unable to solve flows, where the density of the jet and initial lower atmosphere are initially the same. However, the dynamic Sc_t model resolves this problem. Such results could also be interpreted as that the underestimation of turbulent diffusion of momentum (μ_t) in regions with possible occurrence of Kelvin-Helmholtz instability, resulting from the basic turbulence model, are compensated by lower values of Sc_t and Pr_t (Tominaga and Stathopoulos, 2007; Tominaga et al., 2008).

Fig. 17 shows the calculated Sc_t field by the dynamic model proposed in the present work. The model proposed in the present work prescribes

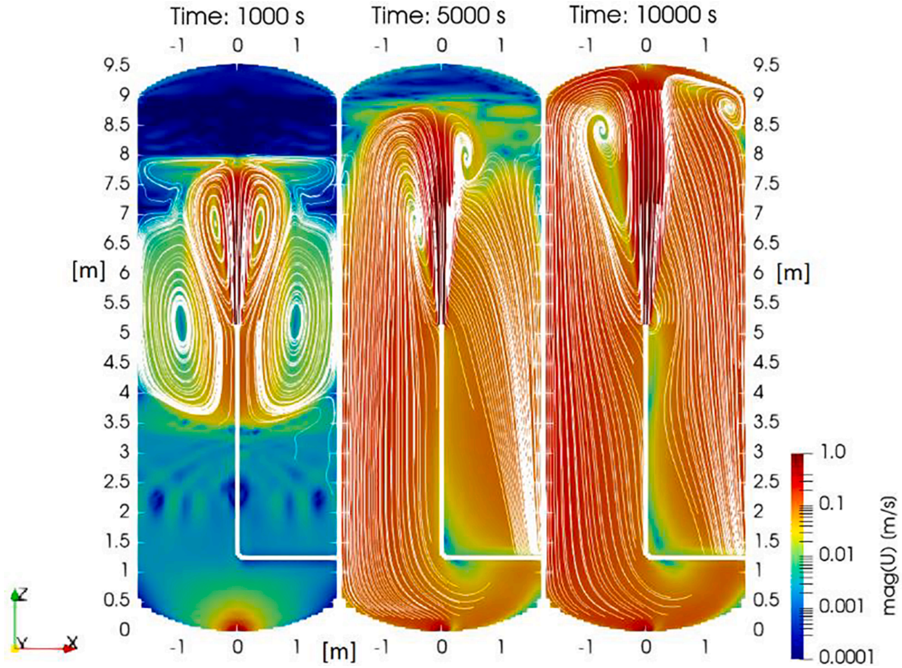

Fig. 14. SPARC experiment: velocity field obtained with proposed dynamic Sc_t model.

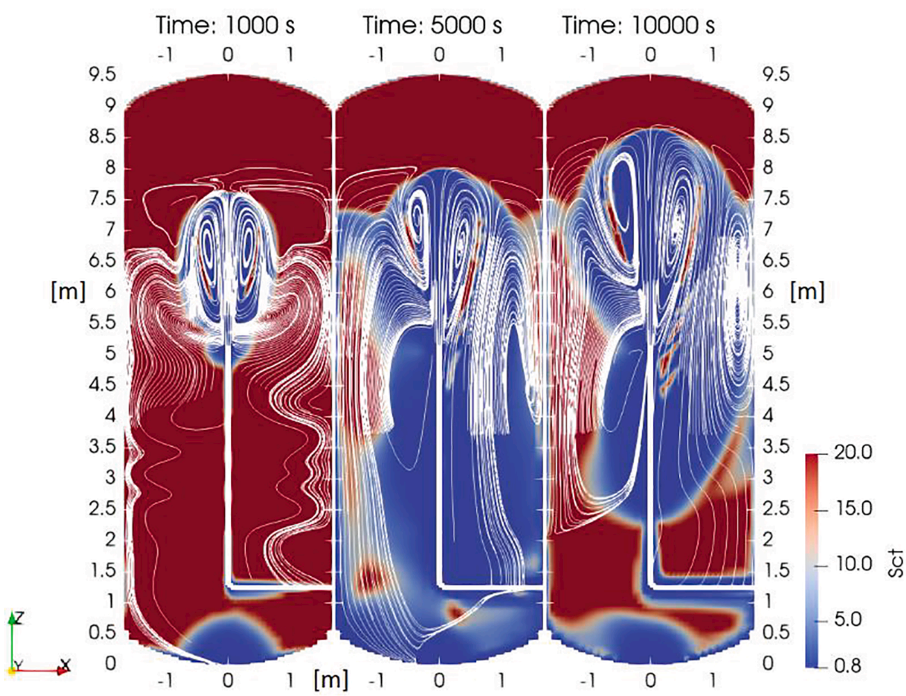

Fig. 15. SPARC experiment: turbulent Schmidt number field given by correlation by Venayagamoorthy and Stretch (2010).

lower Sc_t value in some regions of the jet, making it in compliance with the findings of Shao and Law (2009), Xu and Chen (2012), and Tahmooresi and Ahmadyar (2021).

Fig. 18 shows regions with lower Sc_t values prescribed by the proposed model (in blue) and by the correlation by Venayagamoorthy and Stretch (2010) (in red). Over the entire transient the same value ($Sc_t = 0.8$) is prescribed in the main upward flowing jet. The lower value is prescribed in the downward flowing returning jet and a higher value is prescribed in the interaction region above the jet by both formulations. However, some discrepancies may be observed. Due to the different higher Sc_t values given by both formulations ($Sc_{t,max} = 0.85$ and $Sc_{t,max} = 20$), the transient process develops differently and different flow patterns are generated. The transient obtained with the Venayagamoorthy and Stretch (2010) formulation is slower and is not in compliance with the atmosphere homogenization process observed in the experiment (Fig. 11).

Regions with negative Brunt-Väisala frequency (N^2) are shown in Fig. 19. The area where lower values of Sc_t number is prescribed is marked with a white line and encloses the negative values of the N^2. Negative values indicate a negative vertical density gradient and

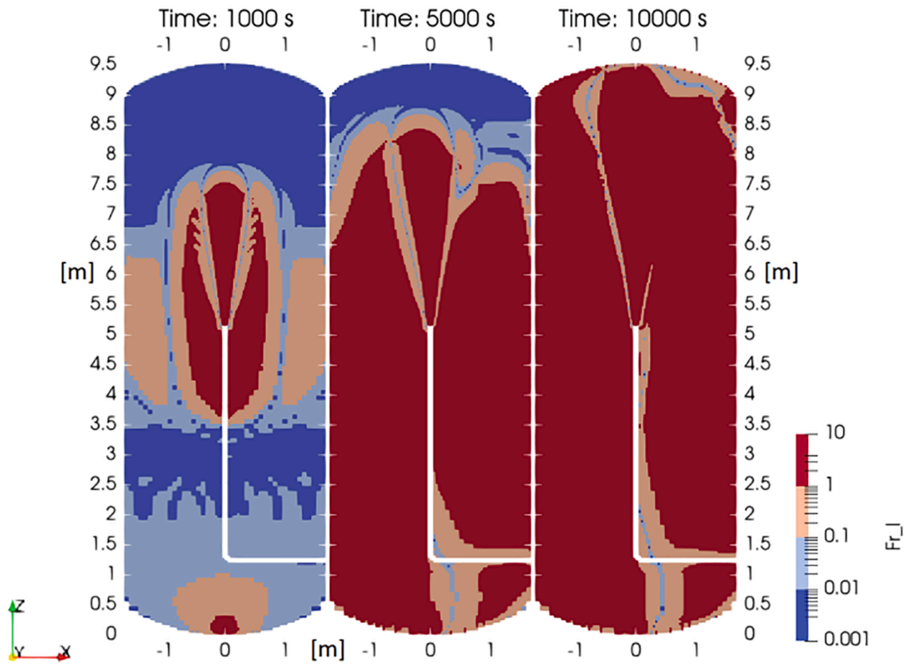

Fig. 16. SPARC experiment: local Froude number.

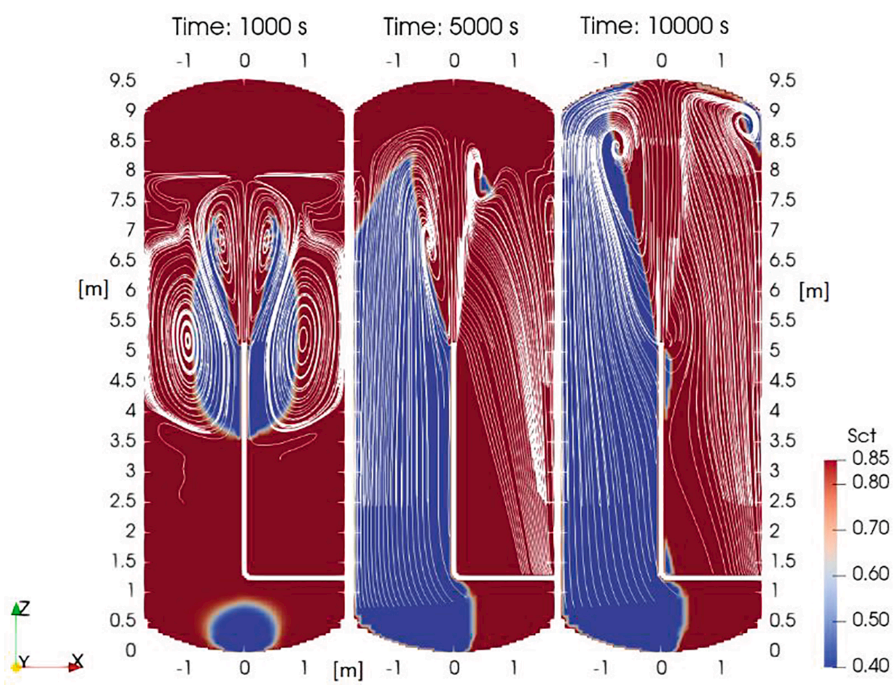

Fig. 17. SPARC experiment: turbulent Schmidt number calculated by the proposed model and streamlines.

unstable stratification. The proposed model maintains a higher Sc_t value in the regions with increasing density stratification and in the interaction region between the jet and light gas layer, and thus does not oppose the Sc_t behaviour given by other studies (Shih et al., 2005), where the value even increases. Furthermore, the negative vertical velocity (in addition to the negative density gradient) also indicates possible occurrence of flow instabilities. First, a Rayleigh–Taylor instability which occurs when the fluid with lower density is below the layer composed of a fluid with higher density, and next also a Kelvin-Helmholtz instability.

Fig. 20 shows the value of D_t (Eq. (12)). The maximal value obtained in calculations at t = 5000 s is $D_t = 0.00925m^2/s$ with the constant Sc_t value, and $D_t = 0.0250m^2/s$ with the dynamic Sc_t model. Discrepancies may be observed between both figures, since due to different Sc_t values prescribed during the transient process, the mixing process develops differently.

5.2. PANDA experiment

Fig. 21 shows time-dependent helium volume fractions at several locations in the PANDA facility, approximately above the injection pipe (figures left) and in the axis of the vessel (figures right). When compared

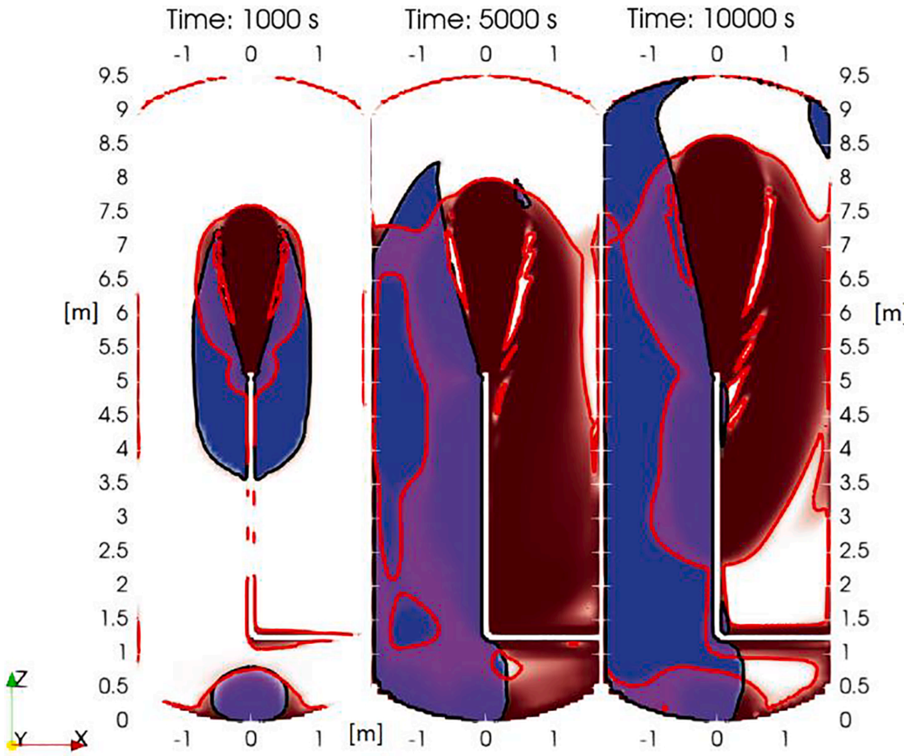

Fig. 18. SPARC experiment: comparison of turbulent Schmidt number fields calculated by both models (blue: proposed model, red: formulation by Venayagamoorthy and Stretch).

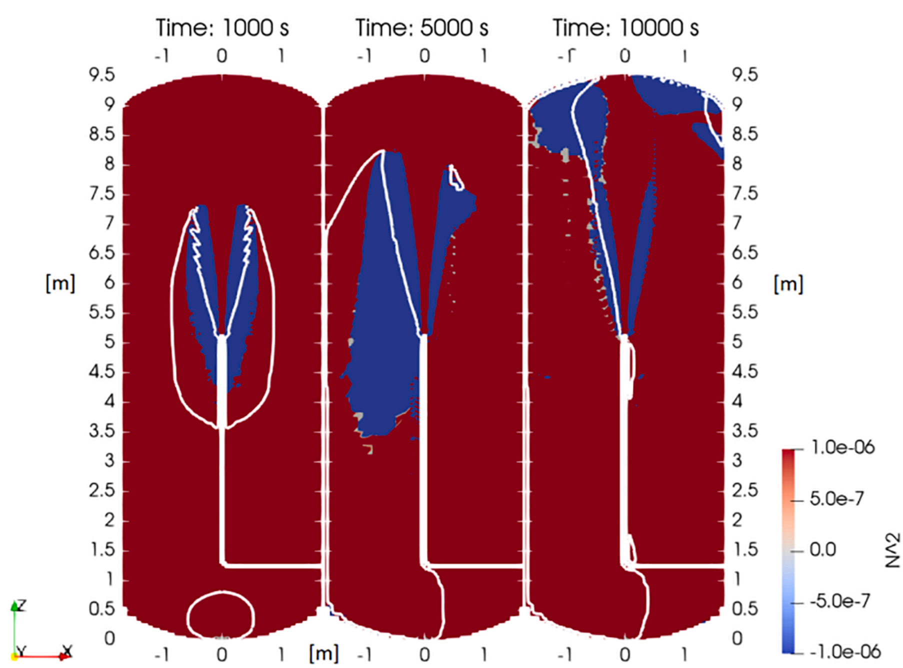

Fig. 19. SPARC experiment: Brunt-Väisäla frequency field (N^2). White line marks the regions with lower Sc_t values prescribed by the proposed model.

to experiment, helium volume fractions in simulations behave similarly, except the values in the simulations are approximately 2 vol% lower. In contrary as it was observed and discussed in the isothermal case in the previous section, there are no discrepancies in the concentration results obtained with constant Sc_t and Pr_t values and the dynamic model.

Fig. 22 shows time-dependent atmosphere temperatures at different locations approximately above the injection (left) and in the axis of the vessel (right). Some discrepancies can be observed between experimental and simulation results (they may appear large due to the scale on the vertical axis). In the upper measuring positions (Fig. 22 top), the temperature in the experiment initially increases steeply, while in the simulations, the atmosphere temperature remains initially constant. Eventually, the temperature in the simulations increases with the same rate as in the experiment, meaning that the turbulent heat transfer from

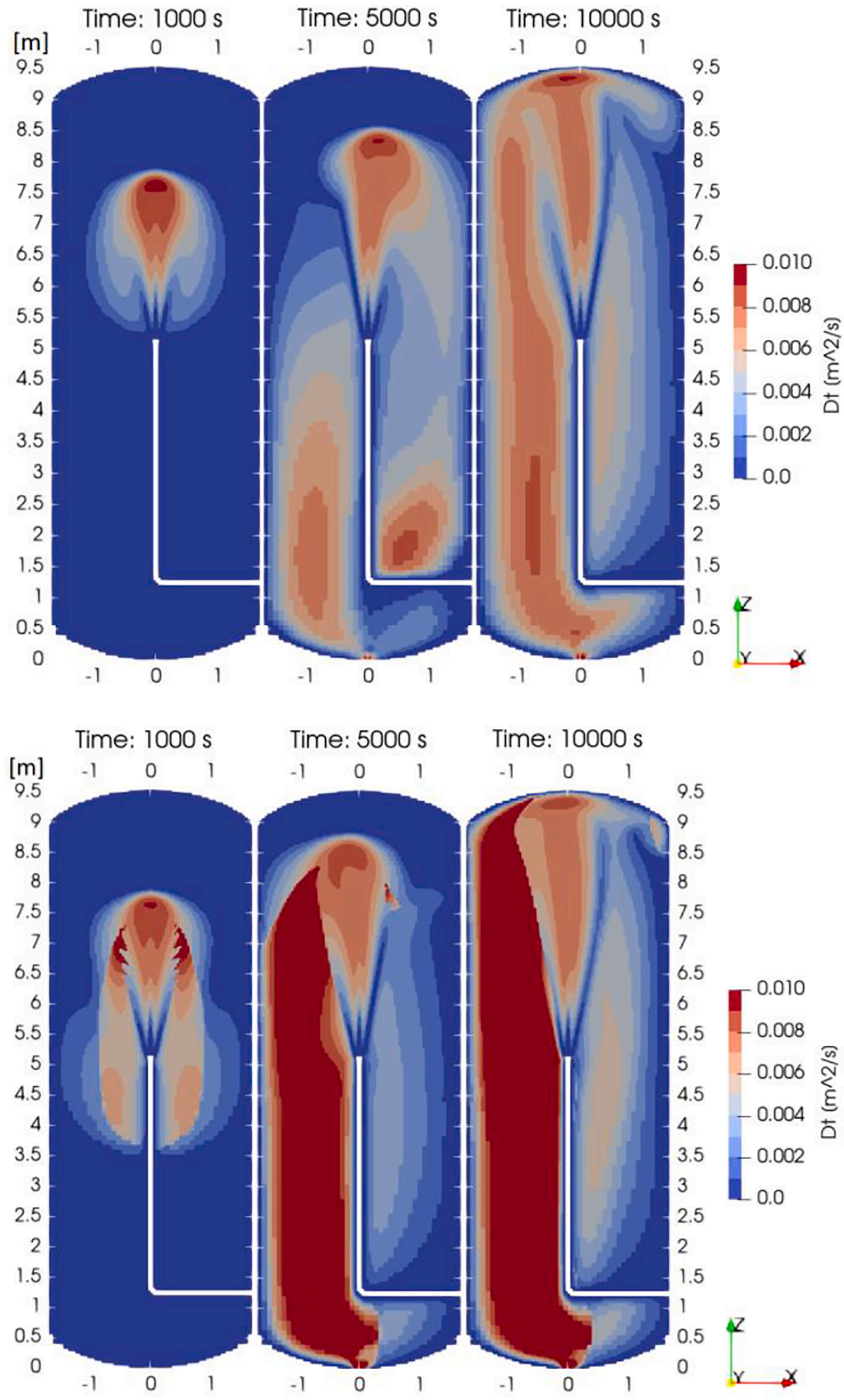

Fig. 20. SPARC experiment: D_t obtained with constant Sc_t value (top) and given by dynamic Sc_t model (bottom).

the hot jet at this point is predicted correctly. Above the inlet (Fig. 22 left), the sudden temperature increase occurs when the top of the jet reaches measuring positions, which happens simultaneously in the simulations and in the experiment. However, despite generally lower temperatures in the simulations, the maximum temperature values in the axis of the vessel (Fig. 22 right), away from the injection, are higher. Later, when the helium layer is fully eroded (after $t \approx 13,000s$), temperatures are generally underpredicted by 2 °C. Similar as in concentration results, there are no discrepancies between the temperature values obtained with constant values and the dynamic model for dimensionless turbulent numbers.

Fig. 23 shows the velocity field measured during the experiment using the particle image velocimetry method (left) and in the simulation with the dynamic turbulent numbers model (right) at t = 5000 s. It can be observed that the jet in the simulation reached the same height as in the experiment; namely the stagnation point (marked with red dot) is approximately at z = 6.35 m in both cases, and also the diameter of the jet is similar.

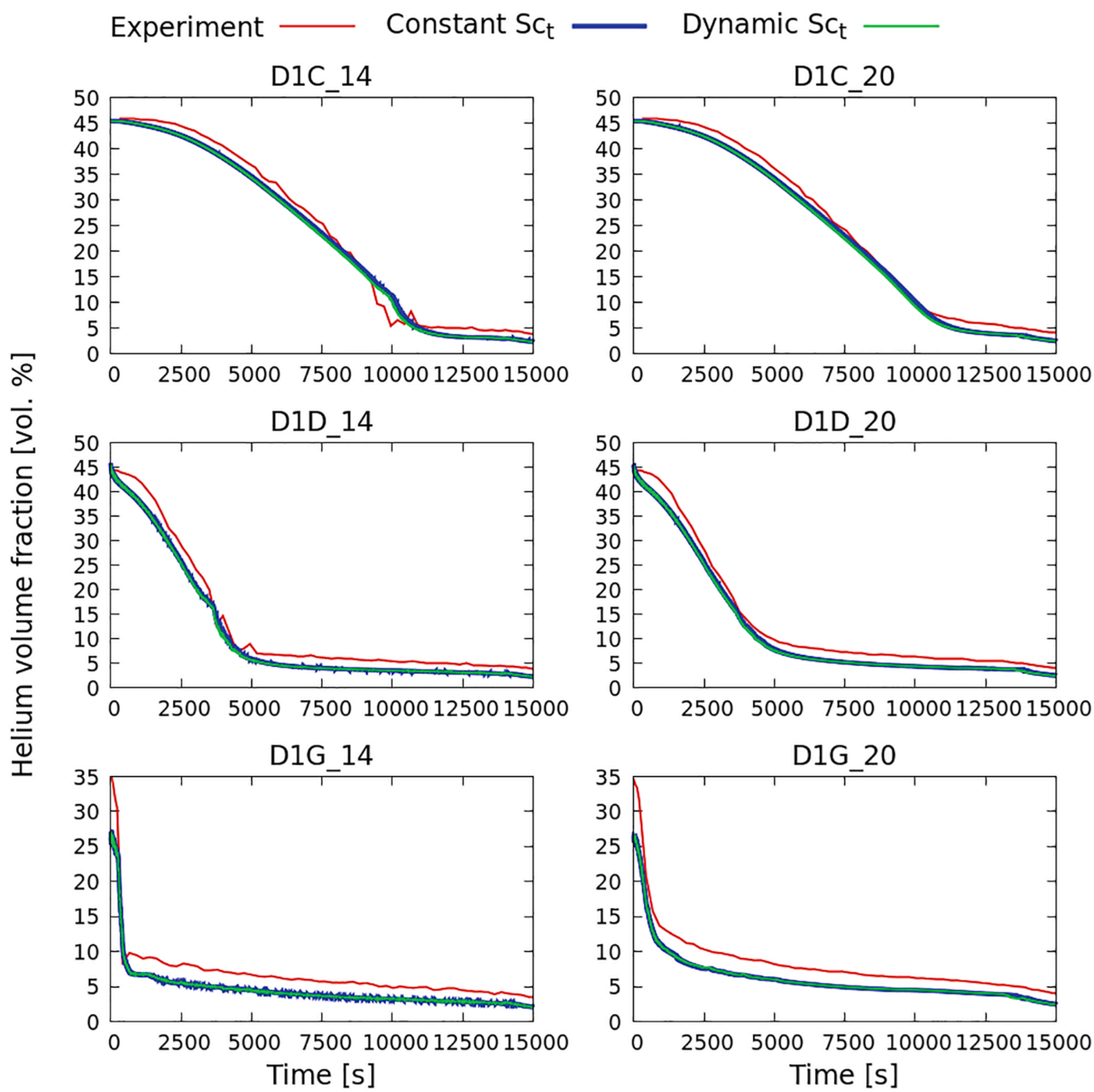

Fig. 21. PANDA experiment: helium volume fraction at different elevations and positions (left: above injection, right: axis of the vessel; for sampling positions see Fig. 7 right).

Fig. 24 shows velocity fields at different times obtained in simulations of the experiment performed in the PANDA experimental facility. It can be observed that a recirculating flow on the left side of the main upwards flowing jet is generated. Fig. 25 shows calculated Fr_l field. $Fr_l > 1$ may firstly be seen only directly above the injection, and on the left side of the main jet with the recirculation region. Only later, when the helium layer is fully eroded, higher values may be observed also in the centre of the vessel and near the wall opposite to the injection. However, during the entire transient, the Fr_l in the proximity of the injection does not exceed $Fr_l = 1$. Since the proposed model takes into account Fr_l and u_z, it does not change the turbulent numbers much until the atmosphere is homogenized (Fig. 26) and thus does not affect the results. Although there is a region with smaller turbulent number values on the left side of the main jet, the results are not affected. The velocity in that region is high and consequently the helium mass fraction is low and the temperature is uniform. Since there are small density and temperature gradients, such small region with lower turbulent numbers apparently does not affect the mixing process.

5.3. MiniPanda experiment

Fig. 27 shows time-dependent helium volume fractions at several locations in the axis of the vessel in which injection occurred. The simulation results obtained with constant Sc_t and Pr_t already agree well with the experimental ones. Due to lower Fr_l (Fig. 30) the dynamic model does not change Sc_t and Pr_t, and its effects are negligible. However, this confirms the basic philosophy of the proposed model, that is, that its results do not differ from the earlier model where the agreement with the experiment is already satisfactory.

Fig. 28 shows time-dependent atmosphere temperatures at different elevations in the axis of the vessel (one should again take into account the scale on the ordinate axis, so the discussion is mostly about small differences). At earlier times, higher temperature values are obtained in calculations in all sampling positions. Later, when the helium layer is fully eroded, temperatures are 2–3 °C lower than in the experiment. The dynamic Sc_t and Pr_t model does not affect the temperature values.

Fig. 29 shows the velocity field at different times in the MiniPanda experimental facility. Fig. 30 shows the calculated Fr_l field in the MiniPanda simulations. A high value of $Fr_l > 1$ may be seen only directly above the injection for the entire transient. Consequently, the proposed

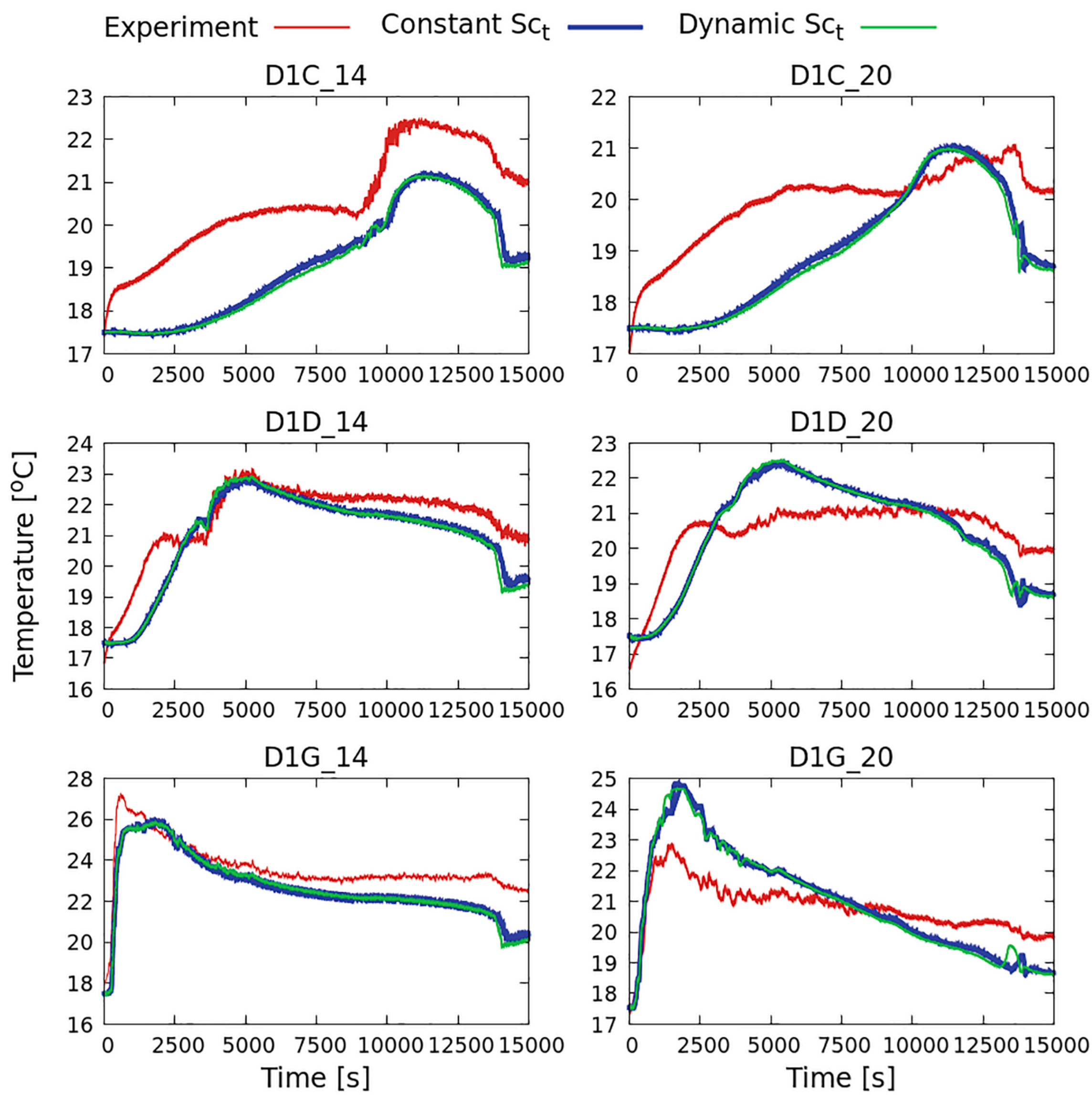

Fig. 22. PANDA experiment: atmosphere temperatures at different elevations and positions (left: above injection, right: axis of the vessel; for sampling positions see Fig. 7 left).

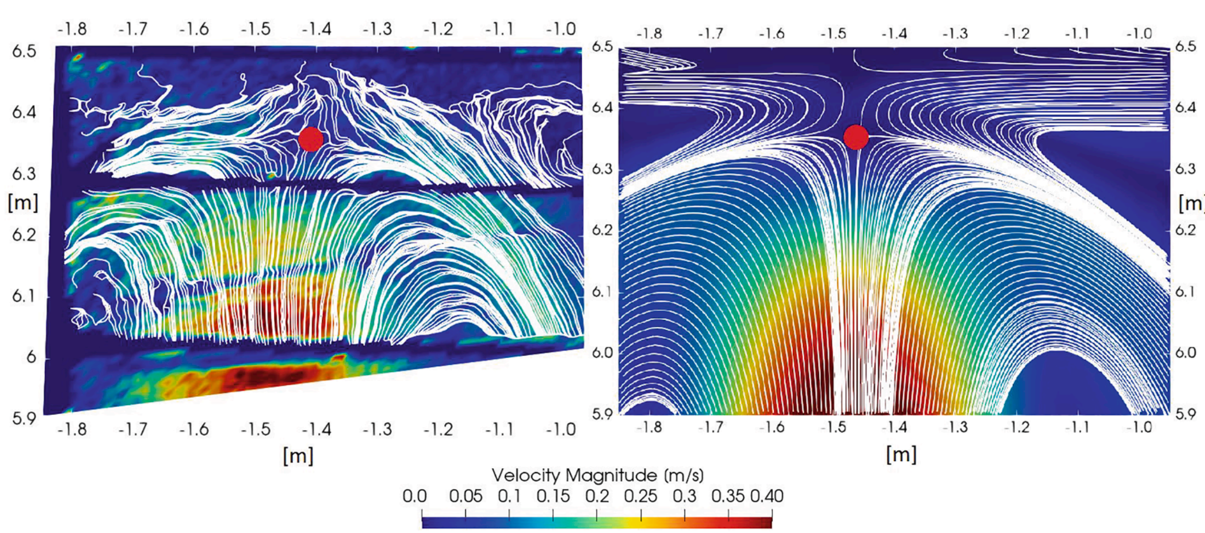

Fig. 23. PANDA experiment: velocity field in experiment (left) and simulation (right) with dynamic turbulent numbers model at t = 5000 s.

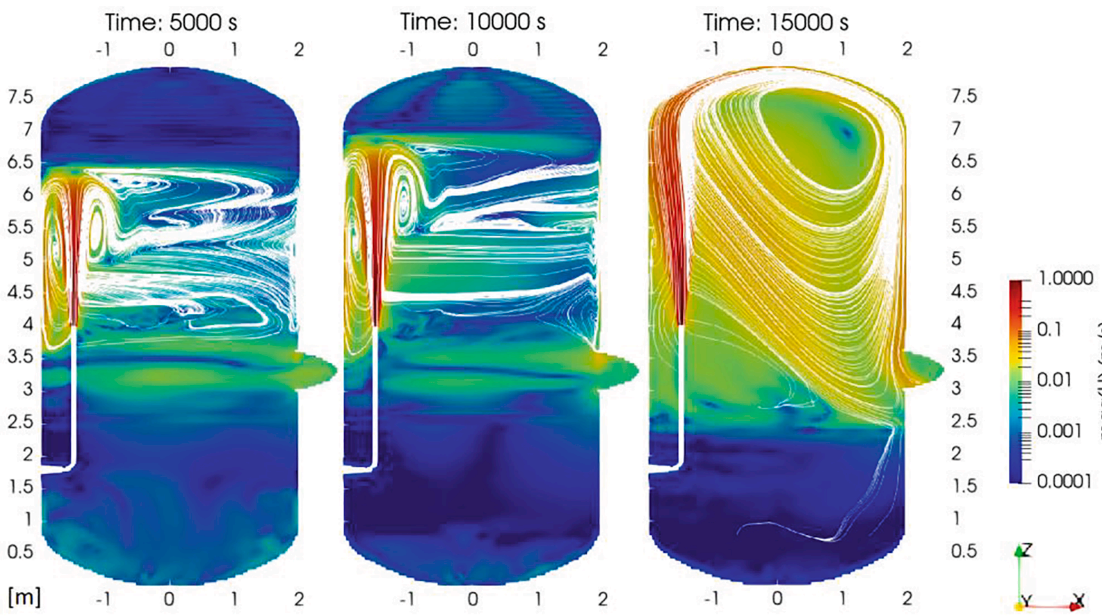

Fig. 24. PANDA experiment: velocity magnitude field.

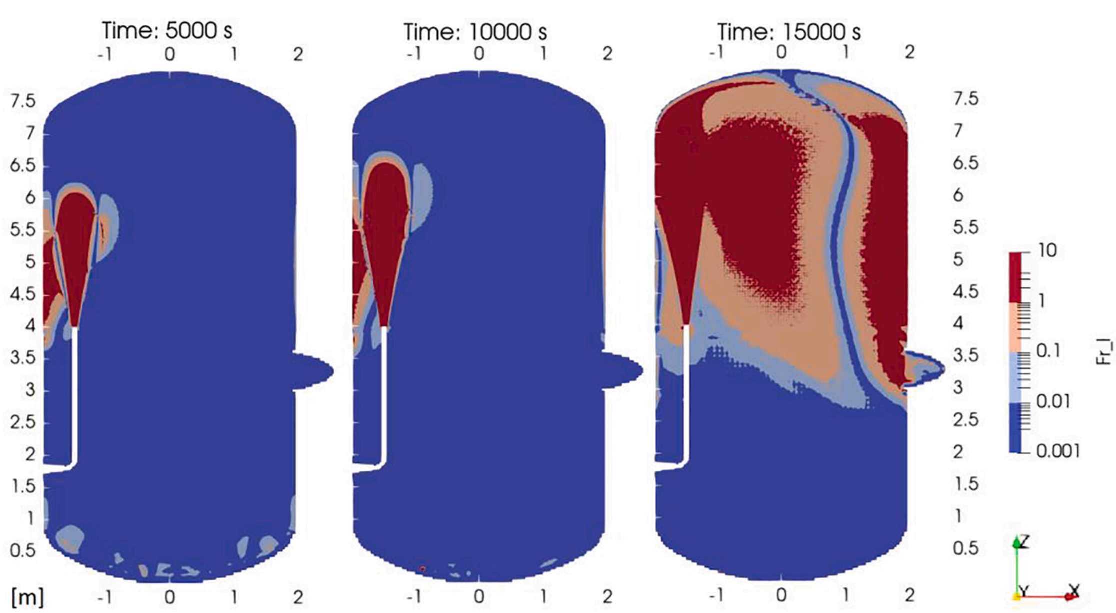

Fig. 25. PANDA experiment: local Froude number.

model changes the turbulent numbers only in very small regions (Fig. 31), which does not affect the results.

The proposed model identifies the regions with possible occurrence of the Kelvin-Helmholtz instability and applies the lower turbulent numbers accordingly. If such conditions are not established during the calculations, the model does not prescribe different values of turbulence numbers and its effects are negligible.

5.4. Last comments

Without Large Eddy Simulations or Direct Numerical Simulations (DNS) of similar cases (similar in terms of Fr_l and possible generation of Kelvin-Helmholtz instability) it is difficult to assess the correct behaviour of turbulence quantities (generation, dissipation, Sc_t and Pr_t). Besides, the atmosphere homogenization with vertical jets is statistically a non-stationary process, which makes it difficult to acquire DNS results with needed accuracy. In some simple benchmarks (backward facing step or single jet), the conditions which would show the drawbacks of the implemented physical model are difficult to achieve. In fluid conditions without possible occurrence of Kelvin-Helmholtz instability, the proposed model does not change the turbulent numbers values and thus does not have any effect.

6. Conclusions

The successful modelling of breaking-up of atmosphere stratification, induced by vertical injection, was extended was extended to isothermal conditions with high mass inflow. With defined local Froude number (Fr_l) the jet behaviour in an environment with a density stratification can be directly characterized during the CFD calculations. The

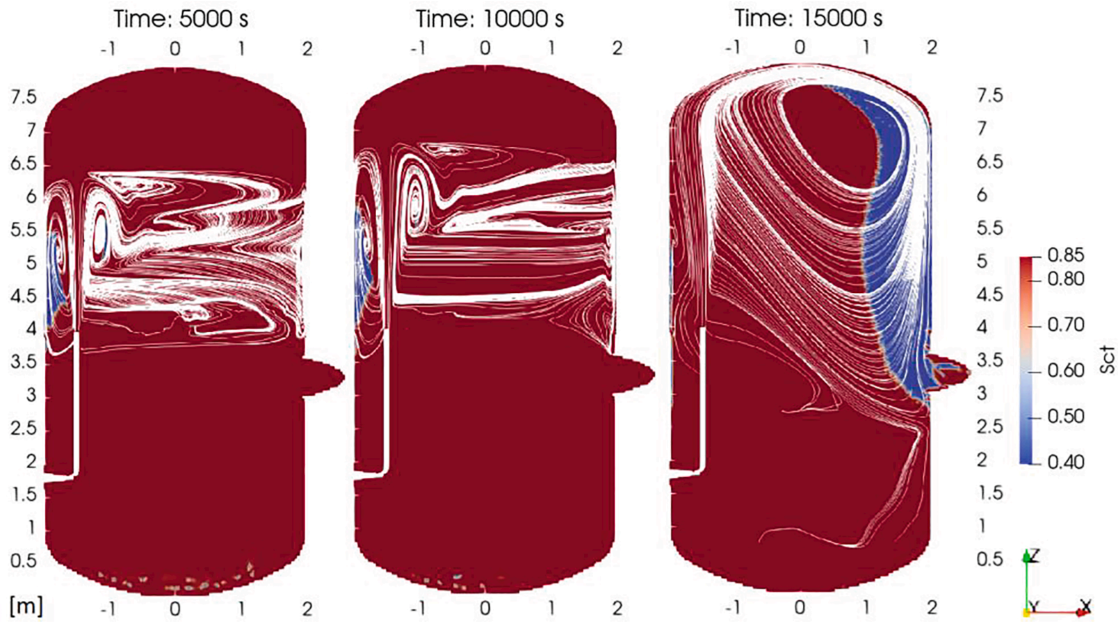

Fig. 26. PANDA experiment: turbulent Schmidt number calculated by the proposed model and streamlines.

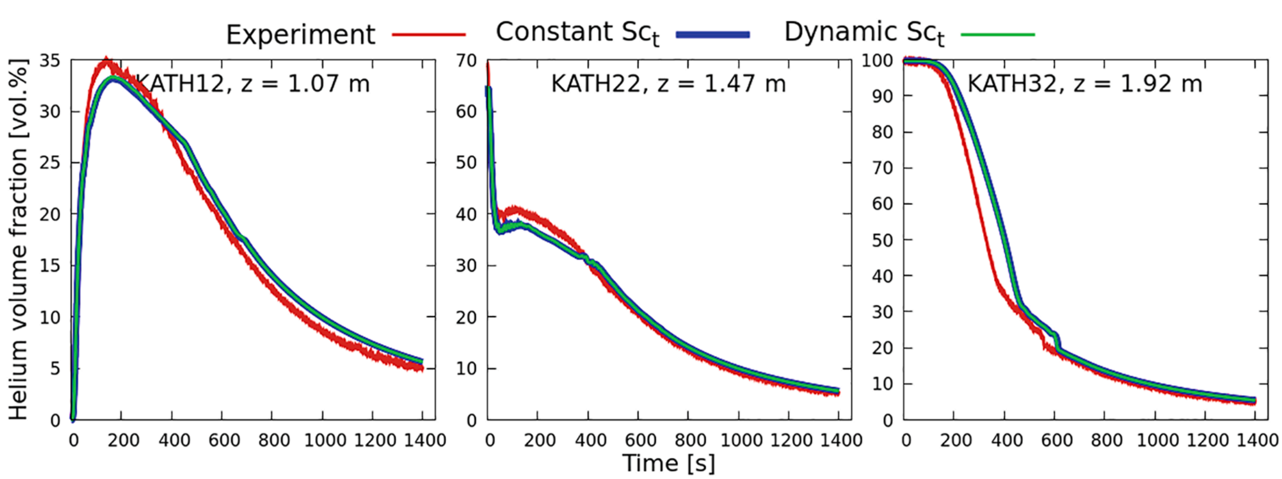

Fig. 27. MiniPanda experiment: helium volume fraction at different elevations in vessel axis (for sampling positions see Fig. 8).

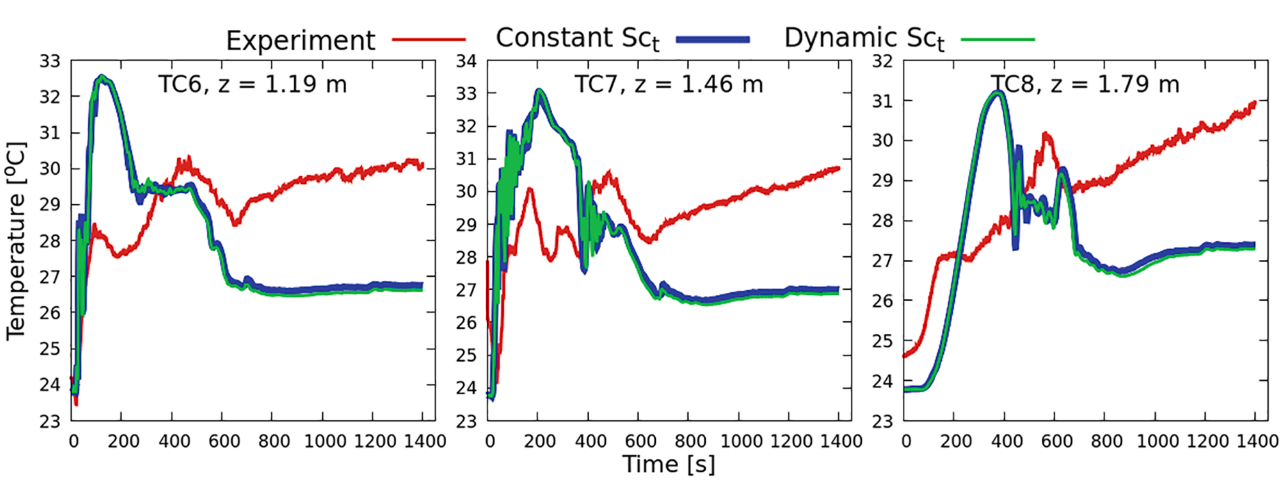

Fig. 28. MiniPanda experiment: atmosphere temperatures at different elevations in vessel axis (for sampling positions see Fig. 8).

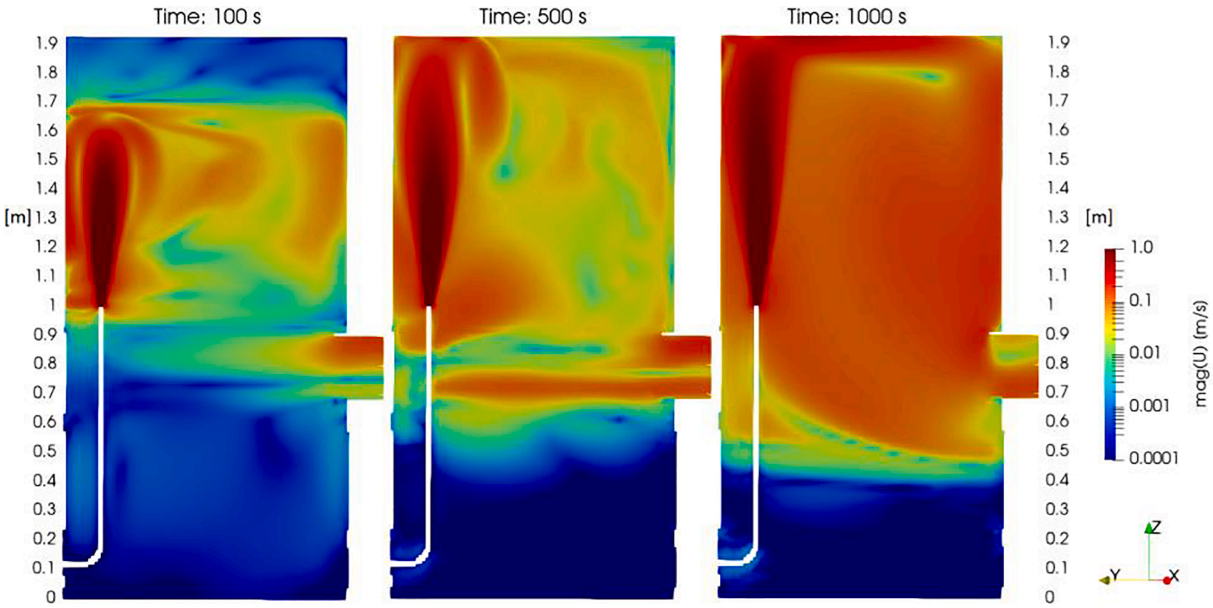

Fig. 29. MiniPanda experiment: velocity magnitude field.

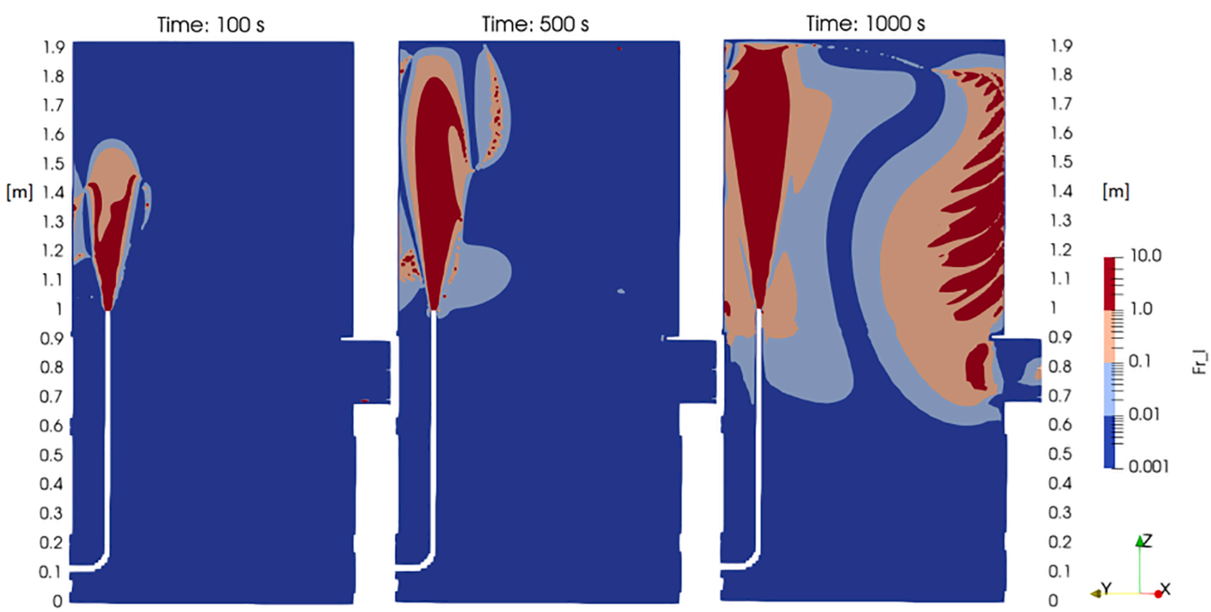

Fig. 30. MiniPanda experiment: local Froude number.

common default physical model (implemented in the OpenFOAM CFD solver) is unable to correctly reproduce the phenomena observed in experiments in which conditions for occurrence of Kelvin-Helmholtz instability are established. The proposed model uses high Fr_l and negative vertical velocity and dynamically prescribes lower turbulent Schmidt and Prandtl numbers to regions with a shear flow and a possible occurrence of Kelvin-Helmholtz instability. The values of the turbulent dimensionless numbers prescribed are in agreement with experimental observations, and do not object to any other studies and models proposed.

The proposed model results in a much better prediction of the experiment performed in SPARC experimental facility, where a light gas layer was eroded by a jet with the same temperature as the previously established atmosphere. On the other hand, the effects of the proposed model are negligible in cases with higher temperature jets performed in PANDA and MiniPanda experimental facilities, where recirculating flow and regions with shear flow are not generated. The proposed model is an extension of the current state-of-the-art turbulence modelling used in simulations of atmosphere homogenization induced by vertical injection and it can be used in any case, regardless of initial and boundary conditions. Namely, the model identifies the regions with possible occurrence of the Kelvin-Helmholtz instability and applies the lower turbulent numbers accordingly. If such conditions are not established during the calculations, the effects of the model are negligible.

CRediT authorship contribution statement

Rok Krpan: Conceptualization, Software, Formal analysis, Investigation, Writing – original draft, Visualization. **Iztok Tiselj:** Conceptualization, Supervision, Writing – review & editing. **Ivo Kljenak:**

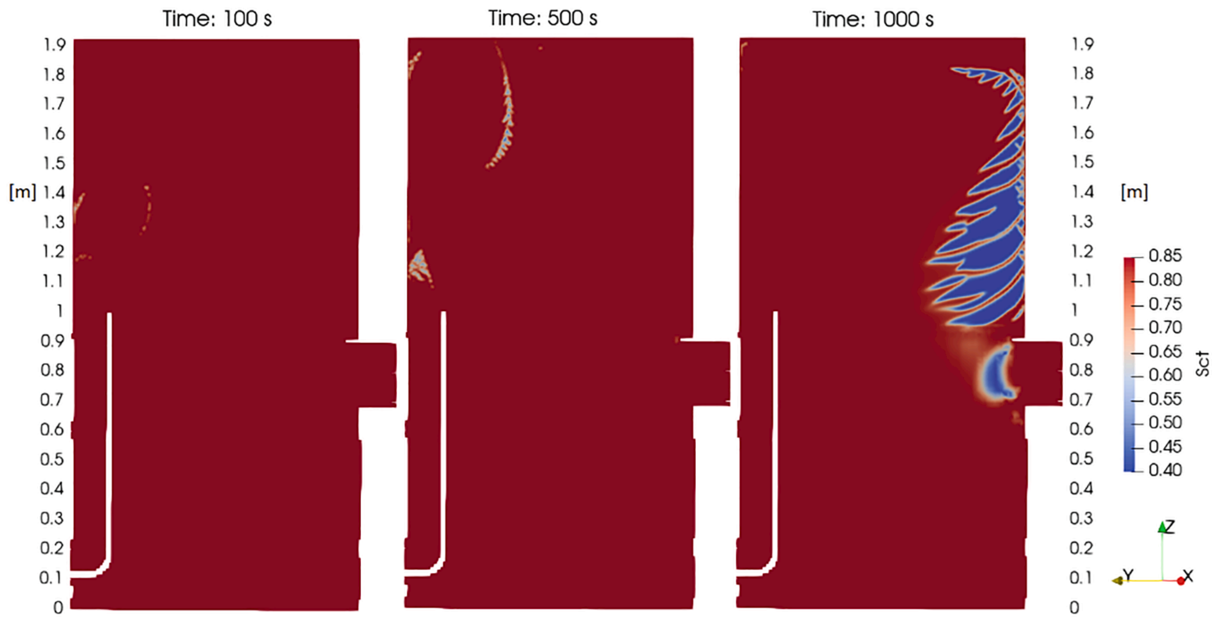

Fig. 31. MiniPanda experiment: turbulent Schmidt number calculated by the proposed model.

Conceptualization, Supervision, Writing – review & editing.

Declaration of Competing Interest

The authors declare that they have no known competing financial interests or personal relationships that could have appeared to influence the work reported in this paper.

Data availability

The authors do not have permission to share data.

Acknowledgments

The authors acknowledge the financial support from the Slovenian Research Agency (research core funding No. P2-0026 "Reactor engineering"). The authors acknowledge M. Ritterath, H.-M. Prasser and the Laboratory of Nuclear Energy Systems at the Federal Institute of Technology Zürich, Switzerland (ETHZ) for providing the experimental data.

References

Abe, S., Studer, E., Ishigaki, M., Sibamoto, Y., Yonomoto, T., 2018. Stratification breakup by a diffuse buoyant jet: The MISTRA HM1-1 and 1-1 bis experiments and their CFD analysis. Nucl. Eng. Des. 331, 162–175. https://doi.org/10.1016/j.nucengdes.2018.01.050.

Abe, S., Studer, E., Ishigaki, M., Sibamoto, Y., Yonomoto, T., 2020. Density stratification breakup by a vertical jet: Experimental and numerical investigation on the effect of dynamic change of turbulent Schmidt number. Nucl. Eng. Des. 368, 110785. https://doi.org/10.1016/j.nucengdes.2020.110785.

Andreani, M., Badillo, A., Kapulla, R., 2016. Synthesis of the OECD/NEA-PSI CFD benchmark exercise. Nucl. Eng. Des. 299, 59–80. https://doi.org/10.1016/j.nucengdes.2015.12.029.

Davidson, L., 2019. Fluid Mechanics, Turbulent Flow and Turbulence Modelling. Department of Thermo and Fluid Dynamics, Chalmers University of Technology, Göteborg, Sweden.

Goldberg, U.C., Palaniswamy, S., Batten, P., Gupta, V., 2010. Variable turbulent schmidt and Prandtl number modeling. Eng. App. Comp. Fluid Mech. 4 (4), 511–520.

Henkes, R.A.W.M., Van Der Vlugt, F.F., Hoogendoorn, C.J., 1991. Natural-convection flow in a square cavity calculated with low-Reynolds-number turbulence models. Int. J. Heat Mass Transf. 34, 377–388. https://doi.org/10.1016/0017-9310(91)90258-G.

Ishay, L., Bieder, U., Ziskind, G., Rashkovan, A., 2015. Turbulent jet erosion of a stably stratified gas layer in a nuclear reactor test containment. Nucl. Eng. Des. 292, 133–148. https://doi.org/10.1016/j.nucengdes.2015.06.001.

Keistler, P., Xiao, X., Hassan, H., Rodriguez, C., 2006. Simulation of supersonic combustion using variable turbulent Prandtl/Schmidt number formulation. In: 36th AIAA Fluid Dynamics Conference and Exhibit, San Francisco, California, USA, June 5–8. American Institute of Aeronautics and Astronautics. https://doi.org/10.2514/6.2006-3733.

Kelm, S., Ritterath, M., Prasser, H.-M., Allelein, H.-J., 2016. Application of the MiniPanda test case 'erosion of a stratified layer by a vertical jet' for CFD validation. Nucl. Eng. Des. 299, 124–135. https://doi.org/10.1016/j.nucengdes.2015.08.013.

Kljenak, I., Bentaib, A., Jordan, T., 2012. Hydrogen behavior and control in severe accidents, in: Sehgal, B.R. (Ed.), Nuclear Safety in Light Water Reactors. Elsevier, pp. 186-227. 10.1016/B978-0-12-388446-6.00003-4.

Koeltzsch, K., 2000. The height dependence of the turbulent Schmidt number within the boundary layer. Atmos. Environ. 34, 1147–1151. https://doi.org/10.1016/S1352-2310(99)00369-6.

Krpan, R., Tiselj, I., Kljenak, I., 2021. Simulations of PANDA and SPARC experiments on containment atmosphere mixing caused by vertical gas injection. Nucl. Eng. Des. 384, 111464 https://doi.org/10.1016/j.nucengdes.2021.111464.

Launder, B.E., Spalding, D.B., 1974. The numerical computation of turbulent flows. Comput. Methods Appl. Mech. Eng. 3, 269–289. https://doi.org/10.1016/0045-7825(74)90029-2.

Lee, W., Song, S., Na, Y.S., Kim, J., 2019. Novel scaling law for long-term interface displacement of a stratified layer by erosion mixing due to turbulent impinging jet applicable to nuclear power plants. Int. J. Heat Mass Transf. 141, 1159–1167. https://doi.org/10.1016/j.ijheatmasstransfer.2019.07.050.

OpenCFD Ltd., 2021, OpenFOAM: The open source CFD toolbox", http://www.openfoam.com/ (accessed 6 May 2021).

Mignot, G., Kapulla, R., Paladino, D., Erkan, N., Zboray, R., Fehlmann, M., Wellauer, C., Bissels, W., 2010. OECD/NEA SETH-2, Vertical Fluid Release Test Series Report. Paul Scherrer Institute, Switzerland.

Na, Y.S., Kim, J., 2018. Introduction to SPARC test facility for assessment of hydrogen behaviour in severe accident. In: 12th Int. Topical Meeting on Nuclear Reactor Thermal-Hydraulics, Operation and Safety (NUTHOS-12), Qingdao, China.

OECD, 2012. SETH-2 Project PANDA and MISTRA Experiments Final Summary Report, NEA/CSNI/R(2012)5.

Paladino, D., Mignot, G., Zboray, R., Fehlmann, M., and Strassberger, H., 2008a. OECD/SETH-2, PANDA Test Facility, Description and Geometrical Specifications. Report TM-42-08-07-0. Paul Scherrer Institute, Switzerland.

Paladino, D., Gupta, S., Mignot, G., Fehlmann, M., Kapulla, R., Strassberger, H., Bissels, W., Ritterath, M., Andreani, M., 2008b. OECD/SETH-2 Project: Definition of PANDA Test Matrix for Low Momentum Vertical Fluid Release at Various Positions. Paul Scherrer Institute, Switzerland.

Ritterath, M., 2012. Instrumentation and Mixing Experiments on Safety Relevant Gas Flows in Containments of Nuclear Reactors. PhD Thesis. ETH Zurich, Switzerland.

Shao, D., Law, A.-W.-K., 2009. Turbulent mass and momentum transport of a circular offset dense jet. J. Turbul. 10 (40) https://doi.org/10.1080/14685240903426505.

Shih, L.H., Koseff, J.R., Ferziger, J.H., Rehmann, C.R., 2000. Scaling and parameterization of stratified homogeneous turbulent shear flow. J. Fluid Mech. 412, 1–20. https://doi.org/10.1017/S0022112000008405.

Shih, L.H., Koseff, J.R., Ivey, G.N., Ferziger, J.H., 2005. Parameterization of turbulent fluxes and scales using homogeneous sheared stably stratified turbulence simulations. J. Fluid Mech. 525, 193–214. https://doi.org/10.1017/S0022112004002587.

Štrubelj, L., Tiselj, I., 2005. CFD Simulation of Kelvin-Helmholtz Instability. Nuclear Energy for New Europe. Nuclear Society of Slovenia.

Sturgess, G.J., McManus, K.R., 1984. Calculations of turbulent mass transport in a bluff-body diffusion-flame combustor. In: 22nd Aerospace Sciences Meeting, Reno, Nevada, USA, January 9–12. Institute of Aeronautics and Astronautics. https://doi.org/10.2514/6.1984-372.

Tahmooresi, S., Ahmadyar, D., 2021. Effects of turbulent Schmidt number on CFD simulation of 45° inclined negatively buoyant jets. Environ. Fluid Mech. 21 https://doi.org/10.1007/s10652-020-09762-6.

Tominaga, Y., Stathopoulos, T., 2007. Turbulent Schmidt numbers for CFD analysis with various types of flowfield. Atmos. Environ. 41 (37), 8091–8099. https://doi.org/10.1016/j.atmosenv.2007.06.054.

Tominaga, Y., Mochida, A., Murakami, S., Sawaki, S., 2008. Comparison of various revised k–ε models and LES applied to flow around a high-rise building model with 1:1:2 shape placed within the surface boundary layer. J. Wind Eng. Indust. Aerod. 96, 389–411. https://doi.org/10.1016/j.jweia.2008.01.004.

Turner, J.S., 1973. Buoyancy Effects in Fluids. Cambridge University Press, Cambridge, 10.1017/CBO9780511608827.

Venayagamoorthy, S., Stretch, D., 2010. On the turbulent Prandtl number in homogeneous stably stratified turbulence. J. Fluid Mech. 644, 359–369. https://doi.org/10.1017/S002211200999293X.

Xu, D., Chen, J., 2012. Experimental study of stratified jet by simultaneous measurements of velocity and density fields. Exp. Fluids 53, 145–162. https://doi.org/10.1007/s00348-012-1275-7.

Yimer, I., Campbell, I., Jiang, L.Y., 2002. Estimation of the turbulent Schmidt number from experimental profiles of axial velocity and concentration for high-Reynolds-number jet flows. Can. Aeronaut. Space J. 48, 195–200. https://doi.org/10.5589/q02-024.